Gas Turbine Laboratory
Department of Aeronautics and Astronautics
Massachusetts Institute of Technology
Cambridge, MA 02139

Final Report on Grant NAG 2321

entitled

CHARACTERIZATION OF AEROMECHANICS RESPONSE AND INSTABILITY IN FANS, COMPRESSORS, AND TURBINE BLADES

submitted to

NASA Glenn Research Center
21000 Brookpark Rd.
Cleveland, OH 44135

ATTN: Dr. George Stefko

PRINCIPAL INVESTIGATOR: Dr. Choon S. Tan
Senior Research Engineer, Gas Turbine Laboratory

PERIOD OF INVESTIGATION: November 1999 – May 2003

August 2003

EXECUTIVE SUMMARY

Wake- and tip-vortex-induced unsteady response on an embedded blade-row in a stator-rotor-stator compressor stage have been assessed using three-dimensional unsteady time-accurate Reynolds-averaged Navier-Stokes numerical simulations. These consists of steady and unsteady wake interacting with a stator blade; unsteady tip vortex behavior on isolated self-induced rotor blade response; steady and unsteady wake interacting with rotor blade with unsteady tip vortex flow behavior; and response of rotor tip vortex to downstream stator. The computations are designed to generate unsteady flow fields that serve to address the following specific technical issues: (1) Conditions/situations for which blade excitations of aeromechanic consequence are to be anticipated; (2) self-induced excitations on rotor blade associated with inherent tip vortex unsteadiness/instability; (3) (resonant) response of rotor blade forced at frequency of rotor tip vortex unsteadiness/instability by upstream unsteady stator wake; (4) conditions for which excitations associated with wakes and tip vortex can effectively persist throughout compressor stages. Computed results for E3 rotor and stator B blade row in NASA Low Speed Research Compressor are presented for (1) illustrating the difference in stator response to an incoming steady and unsteady wakes; (2) identifying and characterizing the inherent rotor tip vortex unsteadiness/instability; (3) demonstrating the potential amplification of response when the rotor tip vortex is forced at its inherent frequency of instability (e.g. by stator wakes from upstream).

Based on the analysis of the computed results, the following observations can be deduced. The self-induced excitations associated with tip vortex inherent instability (at a frequency of 0.45 Blade Passing Frequency) can be considerable and its interaction with other inlet disturbances such as unsteady wakes play a role in the broadening and selective amplification of the spectrum of wakes. The frequency and structural content of the tip flow region are also described; the interface separating the low-momentum tip region from the core flow exhibits a wave-like oscillation which proceeds downstream at a velocity of 0.42 times the core flow velocity at a reduced frequency (based on blade chord and throughflow velocity) of 0.7 (0.45 Blade Passing Frequency). The tip vortex core also exhibits a periodical motion at a frequency of 1.15 BPF. It has been observed that the tip vortical structure is definable in the first 40% chord. Beyond that point, the tip region is a region of low-momentum flow. From the computed flow fields it cannot be conclusively deduced if it is the tip vortical structure or the region of low-momentum flow that is responsible for the observed flow unsteadiness.

When the upstream incoming wakes are fluctuating in strength at a frequency/frequencies (i.e. the wakes are taken to be inherently unsteady; this is to be differentiated from unsteadiness associated with blade row relative motion) other than blade passing frequency and tip vortex instability frequency (in rotor blade rows), new high frequencies - resulting from the mutual modulation of distinct disturbances - can be generated and transmitted downstream within the generated wakes. In both stator and rotor blade rows, it is found that the distinct frequencies independent disturbances can under appropriate conditions exacerbate the resulting interactions. This has the

implication that the influence of unsteady wakes can persist throughout the compressor stages.

When the fluctuation frequency of incoming wakes equals the tip flow instability frequency, no resonance appears as was originally conjectured. The lack of resonant response is presently attributed to the fact that the spatial modal structure of the specified wake is different from that of the tip vortex instability.

In summary the computed results show: (1) rotor tip vortex instability/unsteadiness at a reduced frequency of 0.7 could be an important source of blade excitations (local as well as downstream blade rows via excitations in rotor wakes); (2) the relevance of wake temporal fluctuations in wake-blade interactions on blade response in amplifying and broadening of frequencies; (3) situations/conditions for which the effect of wakes and tip vortex can persist in multistage environment; (4) consideration of blade forced response should include tip flow unsteadiness and interactions with upstream fluctuating wakes/vortices; and (5) sources of potential excitations of the asynchronous types associated with wakes and tip vortices.

Many key technical aspects and results from this research have been presented at the *Seventh National Turbine HCF Conference* May 2002 as well as distributed to the *GUIDE Annual Workshop* August 2002.

Empty page

Contents

List of Figures

List of Tables

Nomenclature

Symbols

Pt Stagnation Pressure

Ps Static Pressure

ρ density

U_{tip} Rotation velocity at rotor tip

$U_{x,inf}$ Axial component of time mean velocity at inlet boundary

X_b subscript b refers the rotor inlet value of physical quantity X

X_c subscript c refers the rotor exit value of physical quantity X

X_d subscript d refers the rotor-stator exit value of physical quantity X

S Entropy normalized by specific heat at constant pressure

$Chord_x$ **or** C_x projection of the (usually rotor) chord on the axial compressor direction

Cp Pressure coefficient are expressed using axial velocity $U_{x,inf}$, thus making them independent from the reference frame

F_x^+ Frequency defined by $\frac{U_{x,inf}}{C_x}$

ΔCp_{s-s} Static pressure rise coefficient

ΔCp_{s-t} Static to Stagnation pressure rise coefficient

Acronyms

LE Leading Edge

TE Trailing Edge

PS Pressure Surface

SS Suction Surface

TV Tip Vortex

CT Convecting time. Time period for a particule to proceed from the inlet plane to the exit plane

NW Refer to the computation case with a uniform inlet flow (No Wake)

SW Refer to the computation case with incoming wakes (Steady Wake)

FWi Refer to the computation cases with a inlet flow containing Fluctuating Wakes. When specified, this acronym might represent the frequency of the wake fluctuation.

RSNW Refer to the computation case with a uniform inlet flow in a complete Rotor-Stator stage (Rotor-Stator No Wake)

TVF Frequency of the spontaneous 'oscillation' of the tip vortex observed in the baseline case NW

LVCF Frequency of motion of the tip vortex core.

freq(s). frequency(ies)

Chapter 1

Introduction

1.1 Background and Previous Work

High Cycle Fatigue failure in gas turbine engines has a significant cost for the US Air Force and Commercial Airline operations. The increased part inventory and frequency of inspection procedures, as well as the inevitable number of related accidents , imply that HCF still constitutes a major technical challenge. One of the key elements to the understanding of these phenomena and the elaboration of preventive designs is structural dynamic loading of blades. Through modern techniques, frequencies and mode shapes are found and classified as one or both of the two classes of excitation: forced vibration and flutter. In gas turbine engines, forced vibration resonance points are determined by the Campbell diagram shown in Figure 1-1 , where the ordinate is frequency and the abscissa is engine rotation rate. The intersection of the n per revolution line with the modal frequency line determines potential resonance conditions for forced response. The designer's aim is to avoid or minimize intersections in the engine operating range and plan for damping to the blades when necessary. In many cases however aerodynamic forcing functions are acknowledged not to be well-predicted nor quantified [28].

As a primary source of excitation of blades, unsteady aerodynamic phenomena appear to be a key element to the prediction of HCF. That air loads are unsteady is well-known and inherent to turbomachines, but discussions at a AFOSR workshop in 1995 [28] emphasize that it remains unclear if all excitation mechanisms have been identified.

The complexity of the flow features in modern, high performance multistage compressors raises the following critical issue: What key physical flow effects must be included in an ana-

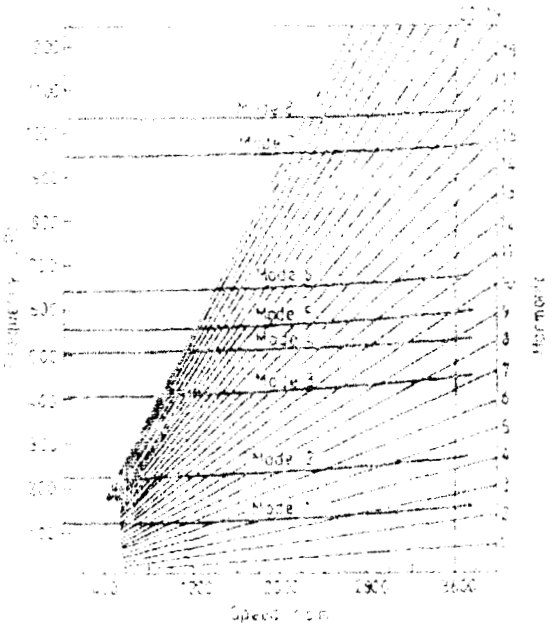

Figure 1-1: Typical Campbell Diagram

lytical/computational model in order to obtain a useful and adequate prediction of unsteady load?

Specific flow situations, formerly considered as secondary, are now being examined for their potential aeromechanical consequences:

- Unsteady Flow separation
- Multi-stage interference
- Tip Vortices in a multi-row environment

The general idea behind multi-stage interference studies is that limited interactions between adjacent bladerows, under appropriate conditions, could lead to a broadening in the frequency band of unsteadiness which might induce significant blade excitations beyond the adjacent blade rows . If this can be shown to be the case, then there is a need to consider the effect of unsteadiness and additional frequencies not only local to a group of adjacent blades but also in other blade rows. The research activity on this broad topic appears to have increased considerably in recent years [18, 24, 4] with computational, analytical [3, 27] as well as experimental [19, 26]

programs. Many other references could be cited here, a good part of which are focused on the development of computational methods particularly suited to address such problems.

Most of the compressor tip clearance flow research that have been carried out were focused on its impact on compressor performance measured in terms of efficiency [2, 11, 8], pressure rise and instability onset [1, 25]. However, its effects on blade forced response have not been examined on a quantitative basis. As mentioned above reliability of turbine engines is nevertheless critical and the studies of tip vortices in the context of multi-stage environment and their impact on blade excitation need to be delineated.

In recent years, experiments have shown the existence of inherent instabilities in compressors under stable operating conditions where compressor instability is not to be expected. This phenomenon, observed in low-speed and high-speed axial compressors as well as centrifugal fans, is believed to be distinct from stall inception and is often referred to as Rotating Instability (RI) by Mailach and al.[13]. It has also been observed in experiments in different axial fans by Mongeau [16], März and al. [14, 15]. It is believed the tip vortex plays a role in its cause, though the mechanism remain unclear. März [14] presumed the periodical interaction of the blade tip vortex with the tip flow of the neighboring blade to be the origin of RIs. More recently, Mailach's experimental observations have shown that periodical interactions of the tip vortex of one blade with the flow at the adjacent blade might indeed be responsible for the generation of RIs. J. Bae [1] has also observed similar large band low-frequency tip flow unsteadiness for large tip clearance gap; he hypothesized that the unsteadiness is associated with the Crow-like instability of the tip vortex and its image in analogy with the pair of trailing vortices downstream of a wing.

In addition to the experimental observations, there have been recent numerical investigations which show the presence of an unexpected spontaneous unsteadiness in the tip flow region. Graf [8] observed such oscillations in the tip vortex pulsing at a 0.5 blade rotating frequency.

Vo [25] during the course of investigating the causal link between tip clearance flow and compressor stall inception, has observed oscillations in the tip flow field for tip clearance gap greater than 2% span. The amplitude of tip vortex periodic (asynchronous) oscillation was noted to increase with the tip clearance size and with increasing stage loading. The frequency was found to decrease with decreasing flow coefficient (0.37*BPF at flow coefficient of around 0.4). The total-to-static pressure rise oscillations near casing could be as large as 10%. Very

early in our numerical investigation, such phenomenon was noted as well, and we chose to focus part of our effort in assessing it.

1.2 Goals and Content of the Thesis

The overall goal of this thesis is to assess and quantify, using computational methods, the role of tip clearance vortices and wakes in forced excitation in the context of interaction with other downstream and upstream sources of unsteadiness representative of a multistage compressor.

Our specific research objectives are as follows:

- Determine the phenomena responsible for and the conditions under which there could be potential transmission and amplification of unexpected unsteadiness across an embedded compressor blade row (rotor or stator).
- Delineate the conditions under which the rotor tip leakage unsteadiness (either self-induced or in its interactions with upstream and downstream perturbations) can lead to blade excitation of aeromechanical consequence.
- Provide design guidelines

To accomplish these objectives, the following research questions need to be addressed:

- What are the conditions under which an amplification of unexpected frequencies downstream of a bladerow can be expected when it is subjected to an unsteady incoming flow such as moving wakes and vortices?
- Could one demonstrate, via numerical simulations, the inherent flow unsteadiness associated with tip vortex that has been observed in the experiments?
- What is the physical origin of self-induced tip vortex unsteadiness?
- What impact do incoming wakes have on this tip unsteadiness?
- Could a wake fluctuation (a third excitation into the system) tuned to match the tip vortex frequency (TVF) exacerbate the impact of TVF on flow characteristics and blade excitation, hence leading to a resonant situation?

- How does the amplitude of pressure field perturbation on the rotor blade surface due to a downstream stator compare to other convected unsteadinesses?

- Based on our findings, what improvements can be made to the design as well as the tools employed for the design of compressors?

- What aspect of this research need further investigation?

1.3 Contributions

The key contributions of this thesis can be summarized as follows:

- The tip vortex inherent instability is identified and the associated blade excitation is found to have a frequency of 0.45 Blade Passing Frequency. Its interaction with other inlet disturbances such as unsteady wakes are found to play a critical role in the broadening and selective amplification of the spectrum of wakes. The frequency and structural content of the tip flow region are also described; the interface separating the low-momentum tip region from the core flow exhibits a wave-like oscillation which proceeds downstream at a velocity of 0.42 times the core flow velocity at a reduced frequency (based on blade chord and throughflow velocity) of 0.7 (0.45 Blade Passing Frequency). The tip vortex core also exhibits a periodical motion at a frequency of 1.15 BPF. It has been observed that the tip vortical structure is definable in the first 40% chord. Beyond that point, the tip region is a region of low-momentum flow.

- When the upstream incoming wakes are fluctuating in strength at a frequency/frequencies other than blade passing frequency and tip vortex instability frequency (in rotor blade rows), new high frequencies - resulting from the mutual modulation of distinct disturbances - can be generated and transmitted downstream within the generated wakes. In both stator and rotor blade rows, it is found that the distinct frequencies independent disturbances can under appropriate conditions exacerbate the resulting interactions. This has the implication that the influence of unsteady wakes can persist throughout the compressor stages.

- When the fluctuation frequency of incoming wakes equals the tip flow instability frequency, no resonance appears as was originally conjectured. The lack of resonant response is

presently attributed to the fact that the spatial modal structure of the specified wake is different from that of the tip vortex instability.

Technical contributions are:

- a full-featured modular user-friendly post-processor has been developed, allowing easy and unlimited analysis to be made from data files produced by J. D. Denton's UNSTREST. This software has been developed using Matlab's APIs and with the investigation of unsteady flow field in mind. It incorporates state-of-the-art data analysis, FFTs and wavelets tools. This effort comprises more than 25000 lines of code and a complete documentation of the data structures used. It is thought to be a very good basis for future investigation.

- through the extensive use of power-spectrum analysis, we have paved the way to an improved consideration of unsteadiness through dual-spectral representations.

1.4 Thesis Organization

The thesis is organized as follows. The overall approach, the numerical tools and the various computations that have been carried out to address the above research questions are described in Chapter 2. Chapter 3 presents the key results from post processing of unsteady computed flow fields in a Stator blade row. Chapter 4 presents the results computed in the case of an isolated rotor subjected to an incoming uniform flow, wakes steady in stator frame and wakes that are unsteady in the stator frames with a range of frequencies different from blade passing frequencies. An unsteady computation of a rotor-stator stage with a uniform inlet flow is also presented. Finally, conclusions and recommendations for future work are given in Chapter 5.

Chapter 2

Approach and Numerical Tools

In this chapter, the flow interactions in multistage compressor is discussed. After delineating the global issues of studying such a system, a strategy of investigation using numerical simulations that focus on a single stage is presented. This stage is subjected to four distinct excitations, which may interact with each other and whose effects will be investigated. These excitations are incoming wakes, fluctuations embedded in wakes, excitation of internal origin - such as tip vortex flow instabilities - and non-uniform pressure field from a downstream blade row. Simulations have been carried out on a stator, a rotor and a rotor-stator stage. The last two sections of this chapter are dedicated to describing each of the numerical setups.

2.1 A Representation of Interaction in Multi-blade Rows Using a Stator-Rotor-Stator Group

In this section, we present the overall problem of inter-blade-row interactions and some of the methods that are used or could be used to investigate the potential impact of coupling in blade-row on aerodynamics and blade excitations. Simulating flow in a multi-stage compressor is a huge computational exercise and as our focus is on carrying specific useful calculations to answer the research questions posed in Chapter 1, a way to decompose the multi-stage problem into single stage configurations is needed. For that purpose, a modular approach is introduced, and one of these modules - a single stage or more appropriately a stator-rotor-stator group - is chosen as the configuration of investigation. How it would fit into a complete model for further investigation is then discussed. Finally, the methodology is described.

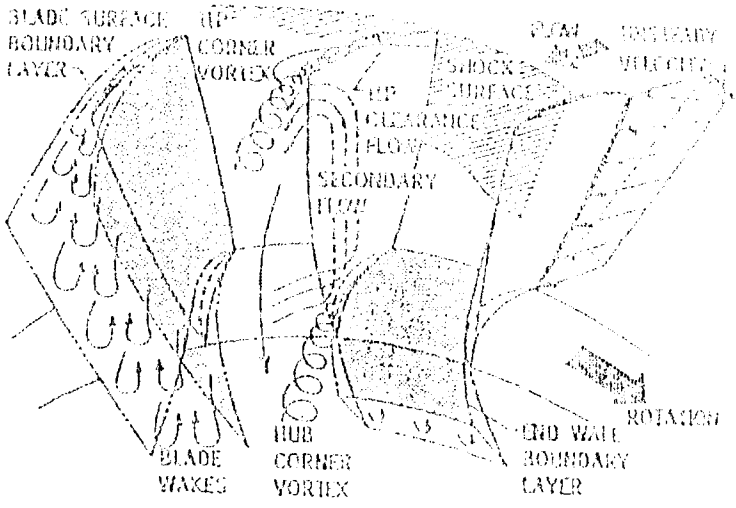

Figure 2-1: The possible range of possible phenomena in a compressor blade row

2.1.1 The added effect of stage interactions

In a single compressor blade row, a wide range of flow phenomena can be encountered as sketched in Figure 2-1 . In an unsteady multi-blade-rows environment, the complexity of the flow field is likely to be much greater due to the multiple interactions between bladerows. Numerous analytical studies of stage interference can be carried out using simplified model of blades, such as lifting lines or using 2D linearized equations; a good number of this analytical approaches can be found in Rao [18]. In such cases, despite a voluntarily oversimplified representation of each blade row, the complexity of the analytical problems has been found to grow dramatically with the number of stage considered.

We can illustrate the potential complexity via the following thought experiment. Consider a bladerow exposed to a steady inlet flow. This blade row generates unsteadiness (e.g. in wakes, tip clearance flow, etc.) which interact with the immediate downstream blade row. Likewise the downstream blade can also be expected to influence the flow in the upstream blade row. Unless there exists some mechanisms to damp out the generated unsteadiness, the blade row beyond the first two would be anticipated to be subjected to the flow unsteadiness generated in the upstream blade rows.

Thus, the following questions can be posed:

- While the influence of a remote blade row would likely be small compared to that of the adjacent blade rows, can it be negligible?

- Could a designer reasonably think that the first rotor, under normal operational conditions, has no relevant effect on the performance and reliability of, for instance, the eighth compressor stage?

A way to synthesize the interactions phenomena in a multistage compressor is to think of them as a modular serial system very much like an electrical engineering problem. This approach is summarized in the next section.

2.1.2 Control-Module paradigm

One could consider a blade row to be a module, which transforms an input (the inlet flow) into an output (exiting flow - downstream) following a transfer function which depends on the geometry of the blade row, the input and some internal oscillator - a flow instability such as that the tip leakage vortex may produce. It is also influenced by a feedback branch coming from the downstream module, the same way it back-influences the upstream module and so forth ...

Figure 2-2 presents a conceptual view of what such a modular model could look like.

As mentioned previously, such analytical studies are possible because the F_i transformation functions are usually taken to be simple. Hence the actual aeromechanical phenomena taking place in blade passages are represented by the F_i functions. Once those functions are known the analysis then only focuses on the inter-blade-row interactions themselves. For instance, in a simplified inviscid approach, the F_i functions might be linear and the module transformation involves a simple transfer matrix as shown in equation 2.1.

$$\begin{bmatrix} \bar{U} \\ \bar{\rho} \\ \bar{T} \end{bmatrix}_{exit} = \begin{bmatrix} \text{3 x 3 transfer matrix} \\ \text{dependent upon} \\ \text{the description of the flow field} \end{bmatrix} \cdot \begin{bmatrix} \bar{U} \\ \bar{\rho} \\ \bar{T} \end{bmatrix}_{inlet} \tag{2.1}$$

where $\bar{U}$, $\bar{\rho}$, $\bar{T}$ are non dimensionalized disturbances of velocity, density and temperature respectively. With L independent variables, a serie of k modules is thus associated with $Lk + L$ variables and a stability analysis can then be applied to the whole systems to investigate the

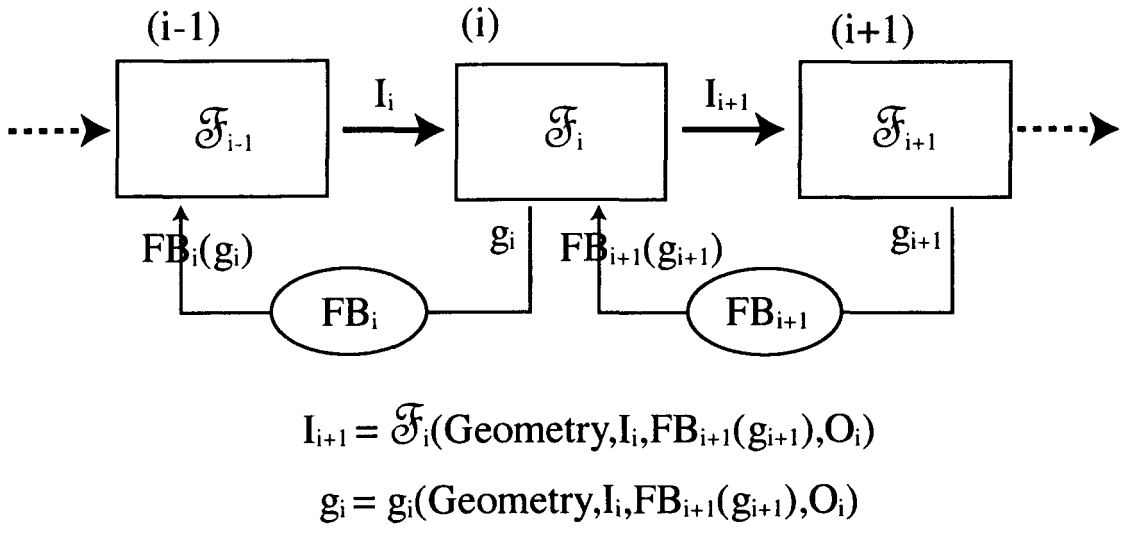

Figure 2-2: A feedback control analysis of blade rows interactions in a compressor

possibility of system instabilities.

As for a control approach, module characteristics can also be expressed in terms of state variables. A more refined description of the flow field through a blade row might give a nonlinear system of equations which might not be solvable analytically but the overall concept remains the same. Such approaches have been partly discussed in [18, 27].

This is what we could call a control-like approach, in reference to electrical engineering methods to deal with intricately systems. It is not intended to try to force the complex Navier-Stokes equations into a over-simplified approach, but just to organize the way bladerows interact, hence focusing on information fluxes - the frequency content for instance - and their transmission between modules.

Consequently, the nature of the information transmitted from one module to other ones and how it relates to the physical reality in a compressor is also a critical question. Since we are mainly interested in the disturbances in the flow field, one might consider to think in terms of power spectrum content instead of physical values, using tools based on wave-number-frequency space instead of physical time space.

For the long term, our primary purpose is to create a low order-model using the concepts described above. A low order model of this nature would necessitate a clear understanding

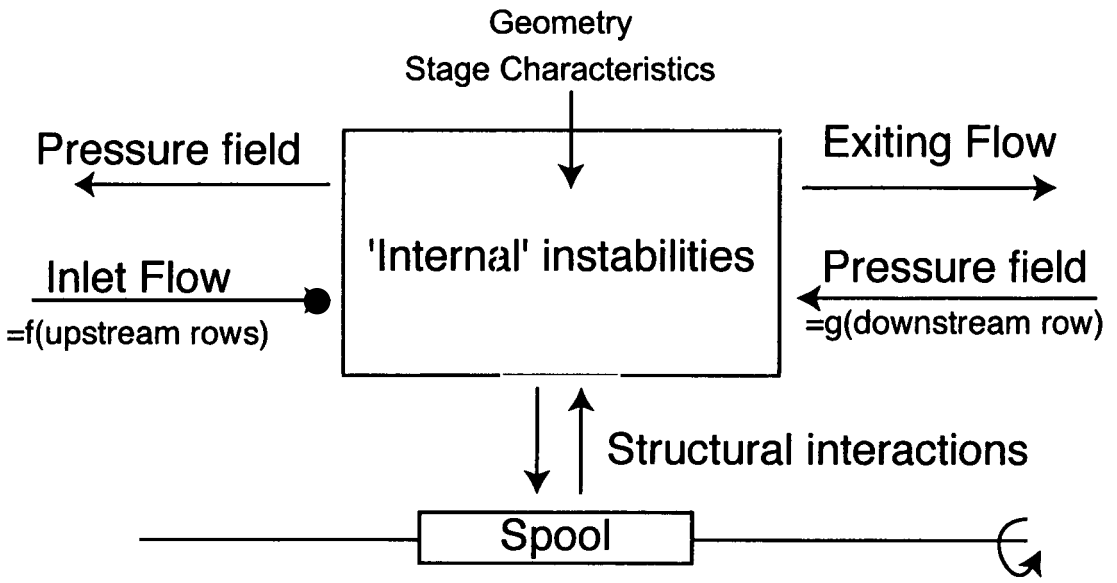

Figure 2-3: A single stage and its connections to the entire compressor

of what might happen in each 'module' - namely compressor stage - thus, our numerical investigation was focused on a single stage and the unsteadiness sources it might be exposed to.

2.1.3 Environment of a single Rotor-Stator stage

Using the GE/NASA E^3 geometry and two different codes for 2D and 3D computations (see sections 2.3 and 2.4), we have focused on the behavior of an isolated stage in a simulated multistage environment.

As sketched in Figure 2-3 , a blade row - either stator or rotor - is obviously influenced by its adjacent neighbors. The downstream influence being mainly the pressure field perturbation associated with the relative motion of the following row. Besides the inlet unsteadiness, internal instabilities such that created by the tip clearance flow (see chapter 4) may bring another source of fluctuation to the system. This lead us to enumerate the unsteadiness source which we will consider in this thesis.

Sources of unsteadiness In this section, we examine the potential sources of flow unsteadiness.

From the inlet flow:

- vortical disturbances, such as wakes and streamwise vortices. Their influence is mainly from upstream to downstream. A wake itself may have unsteady features which could be associated with the design characteristics of the previous blade row as well as its inlet flow conditions.
- pressure field disturbance, such as that due to the presence of a downstream blade row (stator or rotor) in relative motion.
- shocks
- turbulence
- acoustic waves disturbances

From the structure (something we will not cover in this study):

- shaft vibration, due to other bladerows flutter or simply natural vibration excited during functioning

Although shaft vibrations could be considered to have a negligible effect on aerodynamics, it might be the only apparent means of having distant bladerows to directly interact. In critical flight conditions close to engine stall, shaft flexion might play an important role. This is left for future investigation however.

The stage itself can also bring internal disturbances. Given the flow conditions, the stage geometry creates 'regular flow features' for a viscous turbulent flow convecting through it, as shown in Figure 2-1 . There is no source of unsteadiness in this flow unless the flow is unstable.

Flow instabilities associated with specific flow features in a blade passage or blade flutter are also potential sources of unsteadiness and hence excitations. A specific situation involving the instability of tip leakage vortex is considered in this thesis.

2.2 Methodology

Time-accurate, Reynolds-averaged, Navier-Stokes simulations were carried out to obtain unsteady solutions at different operating conditions. The unsteady response of a stator to incoming rotor wakes was addressed using a set of 2D computed results obtained by Valkov [22, 23]

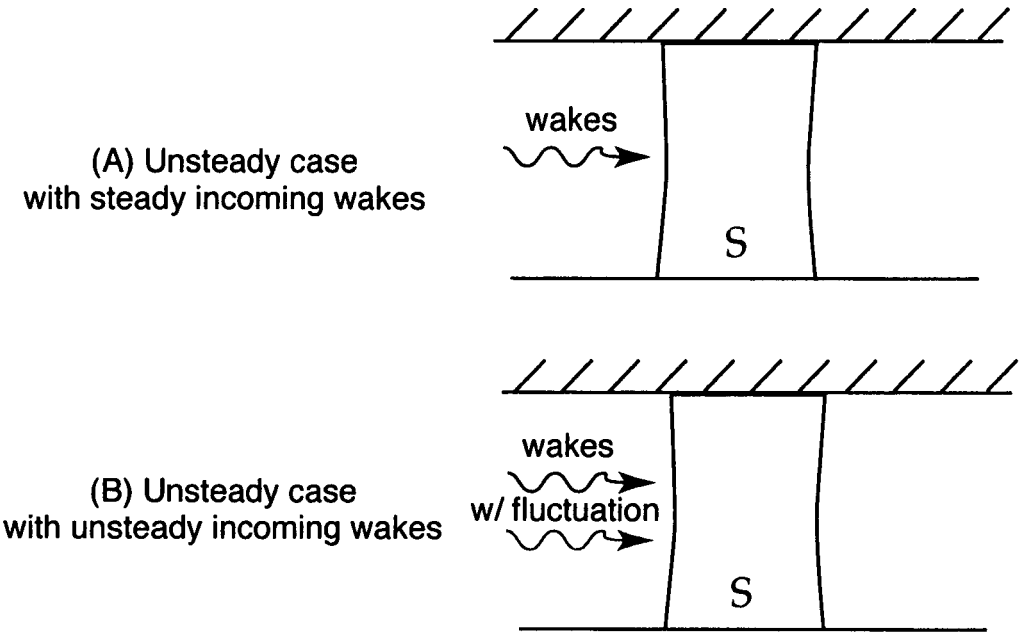

Figure 2-4: The different cases computed on the stator blade row

for Stator B profiles of the E^3 GE/NASA compressor. In his computed results, he considered (see Figure 2-4):

- a situation where the wake is assumed steady in the rotor frame (A)
- a situation where the wake is unsteady and whose strength fluctuates at a frequency other than the blade passing frequency (B)

These results were postprocessed to find out the difference in unsteady response of the stator subjected to wakes steady or unsteady in the rotor frame.

In addressing the rotor unsteady response associated with the tip clearance flow behavior, three situations were considered (see Figure 2-5):

- an isolated rotor where the tip leakage vortex has been hypothesized to exhibit a self-induced instability (A)
- the interaction of a rotor with incoming stator wakes for determining the response of tip clearance flow (hence the resulting unsteady rotor blade response) to variation in the frequency of the stator wake fluctuation (B,C)

- an isolated rotor-stator stage for determining the influence of the downstream stator on the rotor excitation (D)

UNSTREST code [5] was used to implement a set of unsteady 3-D simulations that enable us to determine the role of the self-induced tip vortex instability, the unsteady wake-tip vortex interaction and of the downstream stator in the unsteady response of the rotor embedded in a multi-blade row environment. The rotor configuration was that of the stage-B E^3 GE/NASA compressor with a tip gap of 3% span. Such a fairly large tip gap was chosen to enhance the effect of the tip clearance flow.

All results for the rotor and stator have been analyzed with the followings in mind:

- an understanding of flow mechanisms involved in the phenomena observed
- assessment of the aeromechanical excitation of blades
- a synthesis of results for evaluating their potential integration in the future development of a low order model of multi-stage interference.

2.3 Stator simulations

As noted previously, these computations were carried out by Valkov and the readers are strongly invited to refer to Valkov's masters and doctoral thesis for further information [22] and [23]. Contrary to other computations referred to in this study, Valkov's computation were taken 'as is' with no modification of any sort from our part. Therefore we will thus remain brief and provide a concise description of those simulations.

A wide set of simulations have been carried out in 2D as well as in a 3D rectilinear stator cascade on the geometry of Stage VII of the NASA/GE E^3 compressor at design point and at higher loading (near stall). The cascade consists of an extruded mid-span profile of Stage VII stator. The results were post-processed to investigate the effect of upstream vortical disturbances such as wakes, tip vortex and streamwise vortices on the resulting excitation of blades (in contrast to Valkov's study which focused on time-average performance).

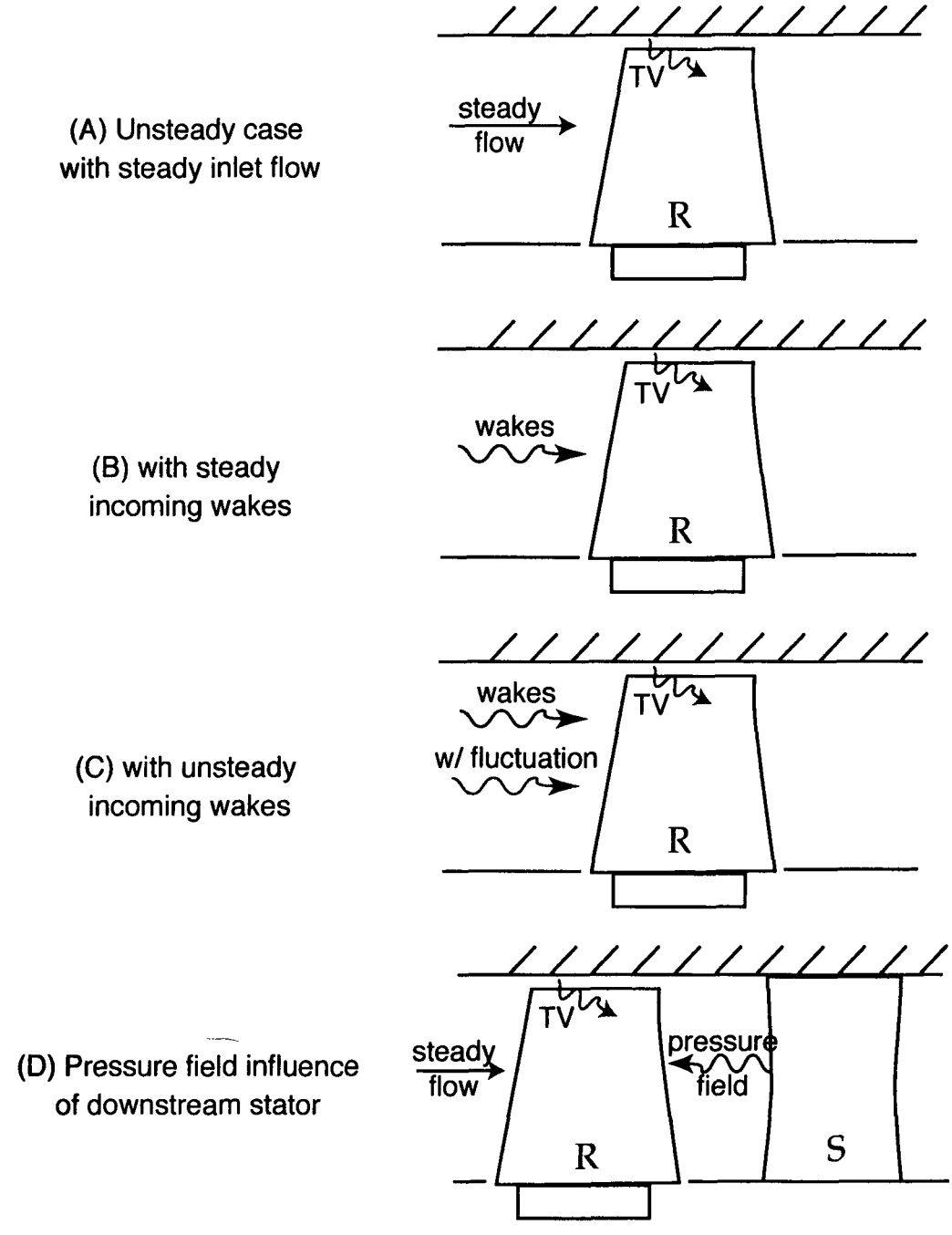

Figure 2-5: The different cases computed on the rotor blade row

	Simulated Stator	Stage VII high-speed Stator
Inlet Mach Number	0.11	0.55
Reynolds	247000	N/A
Stage Reaction	63%	68%
Hub/Tip Ratio	0.85	0.89
Solidity	1.67	1.67
Aspect Ratio	1.34	1.37
Stagger	32	N/A

Table 2.1: Main stage characteristics

2.3.1 Presentation of the code

The computational procedure is based upon a spectral element method which can be considered as a hybrid method of a finite element method (Girault 1986, Hirsch 1988 [6, 9]) and a fully spectral method (Gottlieb and Orszag,1977 [7]). This method divides the computational domain into a number of regularly-sized regions. A high-order expansion of the flow field within each region is carried out, thus achieving both geometric flexibility and high accuracy. The base algorithm was developed at MIT by Patera (1984) and Korczak (1985) [17, 12] for 2D laminar flows. It has since been modified to allow the representation of turbulent unsteady 3D flows until the mid 90's (Renaud 1991, Valkov 92 [20, 22]). The 3D code consists of a spanwise eigenvalue decomposition allowing the representation of 3D internal flows as a series of independent two-dimensional problems in modal space. The code uses a modified Baldwin-Lomax model of turbulence. The mesh is H-structured and each element contains 7*7 nodes.

All the results were from single passage calculations, both for the 2D situation and for the 3D rectilinear cascade setup.

2.3.2 Geometries and Flow Conditions

The geometry is an "Aerodynamically scaled" model of Stage VII of the NASA/GE E^3, 23:1 pressure ratio compressor - Low Speed Research Compressor (LSRC) . Aerodynamically scaled meaning that the simulated model tend to reproduce the flow conditions in the row but at lower speed (see reftabtab:stagecharacteristics)

The tip vortex strength was chosen to correspond to a 3% tip clearance as opposed to the actual 1.8% of E3.

	Design Point	High-loading point
Flow coeff.	0.45	0.38
Stage pressure coeff.	0.65	0.73
Stage inlet air angle	46	50.7
Stage exit air angle	21	N/A
Stator diffusion factor	0.41	0.51

Table 2.2: Main parameters of two flow configurations

Two operating points were simulated: design point and a high-loading point.

The axial spacing was also implicitly represented by the amplitude of the velocity defect in the wake; it has been chosen in the range of 0.07 to 0.37 chord. This reduced spacing is aimed at exacerbating the effects of the incoming disturbances. The domain inlet boundary is 0.185 chord upstream of the leading edge, the rotor-stator blade count ratio has been chosen equal to 1:1.

2.3.3 Input Flow - Boundary conditions

This section describe how wakes, tip vortex and streamwise vortex have been simulated as moving velocity disturbances superposed upon the steady flow on the inlet boundary of the computational domain.

Wakes

The upstream wakes are represented by a symmetric two-dimensional Gaussian profiles of velocity defect in the rotor frame. For the sake of simplicity, the velocity defect has no radial component and the velocity defect Δu is chosen to be parallel to the overall flow direction in the rotor frame. The stagnation pressure depends on an amplitude parameter A_d and a width parameter w:

$$P_t = P_{unif} \cdot (1 - A_d \cdot \exp(-(\frac{2 \cdot (y - y_r)}{w})^2)) \tag{2.2}$$

where y_r is the tangential position of the maximum defect, w controls the width of the wake, A_d is the relative amplitude of fluctuation, P_{unif} is stagnation pressure of the uniform flow and

P_t is the stagnation pressure including the wake defect

The fluctuation of the amplitude parameter A_f has a monochromatic form:

$$A_f = 1 + A_{amp} * \sin(2\pi \cdot \frac{t}{T_{fluct}}) \tag{2.3}$$

where T_{fluct} and A_{amp} are the period of the fluctuation and relative amplitude of fluctuation respectively.

2.4 Rotor 3D simulations

2.4.1 Numerical code

Time-accurate computations have been carried out using UNSTREST, developed by Denton of Cambridge University. It is a second-order code which makes use of a distributed body force to simulate viscous effects. UNSTREST uses a simple mixing length turbulence model. A value of 0.05 mid-span pitch has been chosen for all blade rows, in accordance with the value chosen by Vo [25]. The exact value is not important since our investigation is focused on trends and unsteady forced response. However, in Figure 2-7 we can note that our computations are in accord with the experimental measurements by Silkowski [21]. The compactness of the code enables efficient computations, hence allowing us to carry out unsteady three dimensional simulations with a refined mesh size on multiple single-passage stage using personal computers. On a 1.2 GHz AMD Athlon PC, a typical generation of unsteady solutions took of the order of several days.

2.4.2 Implementation of blade row geometry

The Rotor/Stator B stage of GE E3 has been used as the primary geometry of our investigation.

It had been observed (appendix D of Vo's thesis) that large oscillations occurred in the tip flow with maximum amplitude around a tip clearance of 3%. The frequency and the extent of these oscillations have been determined to be due to a numerical artifact (Vo [25]) but to some interaction of the tip clearance flow with the main core flow.

A duct was used upstream of the rotor stage to generate the incoming wakes. This duct, placed in the absolute frame, was truncated so as to limit the computational time penalty

Parameter	IGV	Rotor B	Stator B
Number of blades	110	54	74
Stagger Angle (deg)	10	50	40
Solidity (mid-span)	1.4	1.16	1.43
Hub-to-tip ratio	0.85	0.85	0.85
Aspect ratio	-	1.17	-

Table 2.3: Design parameters of the GE LSRC

implied by its presence and to match its inlet boundary with the trailing edge axial position of the IGV of the real E3 compressor. As explained later, the wakes generated at the inlet of the duct were set the minimal velocity within the wake is zero. This was chosen so that the inlet boundary can be interpreted as coinciding with the NGV tailing edge position.

The typical size of the meshes used is 140*50*50 for the single-passage duct-rotor configurations and up to 210*50*50 for the single-passage duct-rotor-stator case (see 2-6).

2.4.3 E3 blading and Flow Parameters

This section is aimed at describing the B-stage of the E^3 geometry, as implemented in our computations. Operating conditions under which we chose to simulate the blade row behavior are also discussed and compared to real-world experimental tests.

Rotor/Stator B stage of the E3 compressor

Simulations have been implemented using the rotor B geometry alone. Figure 2-6 shows different views and perspectives of the geometry, the shape of the domain and the grid mesh. The geometry data has been provided by B.F. Beacher of GE company.

The main geometrical parameters are summarized in Table 2.3 . For sake of simplicity, a 1 to 1 blade ratio has been chosen between IGV and and rotor. Ducts generating wakes have thus the same pitch periodicity as rotor passages. For the complete rotor-stator implementation, a 54:74 has been kept has it is critical to identify the pressure field effect of downstream stator on the rotor excitation, the tip vortex behavior and the associated frequencies.

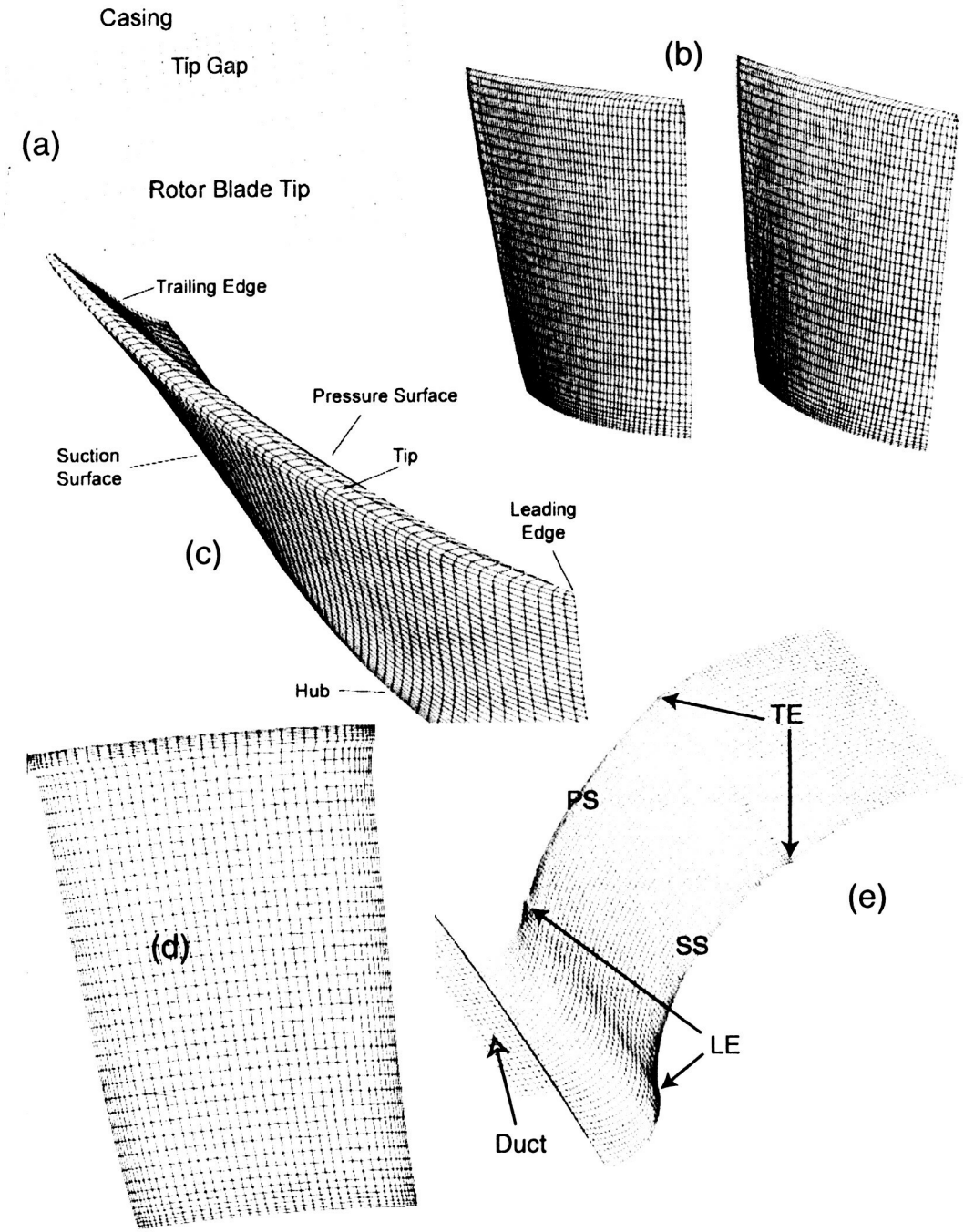

Figure 2-6: Overview of the grid used for E3 B rotor geometry. (a) shows an axial cut of the grid in the vicinity of the tip gap; (b,c) show the shape of rotor blades; (d) shows an entire axial cut of the grid; (e) is a perspective of a radial cut of the single-passage grid with duct and rotor bladerow

Details on the different computed configurations

In all cases, the inlet flow was predefined to match the expected total pressure, stagnation temperature, flow angle and meridional pitch angle at exit of E^3 IGVs. Static backpressure near casing at exit of each bladerow - rotor (and stator if applicable)- is then set as a requirement. The program then precalculates an estimate backpressure distribution at exit of each blade row from the value at casing through a radial equilibrium approximate equation. This pressure distributions are used to generate an initial conditions to allow the advancement of unsteady Navier-Stokes equations forward in time.

The cases considered are the followings:

- Duct-Rotor with no wake (NW)
- Duct-Rotor with steady wake (SW)
- Duct-Rotor with fluctuating wake (FW1,FW2, FW3, FW4)
- Duct-Rotor-Stator with no incoming wake (RSNW)

In RSNW case, stator backpressure was chosen so that the flow coefficient and rotor backpressure could match the rotor-only NW case. Again, the inlet flow was designed to be the same.

Peter D. Silkowski [21] carried out a series of experiments on GE/NASA E3 LSRC, providing pressure rise characteristics for the B stage with a tip clearance Gap/Span of 3.1%. We have used this characteristics graph as a basis to determine how our various numerical computations compare. Figure 2-7 shows this comparison.

These experiments provide data on the entire stage and it has been necessary to estimate the expected stagnation to static pressure rise coefficient for the rotor-only computations. This estimation process is detailed in the Appendix A.1. As shown, these estimates are in accord with the experimental data. NW is slightly above the measured characteristic, this could be due to our omission of the IGV wakes. SW on the contrary is under the experimental curve, which suggest that the stronger wakes created slightly overcompensate the lower solidity of our simulated IGV (54 blades versus 110 in the actual case). We also note the significantly lower flow coefficient of the FWi cases compared to NW, due to the velocity defect implied by the wakes themselves. One of our main preoccupations was to ensure that all FWi and SW have

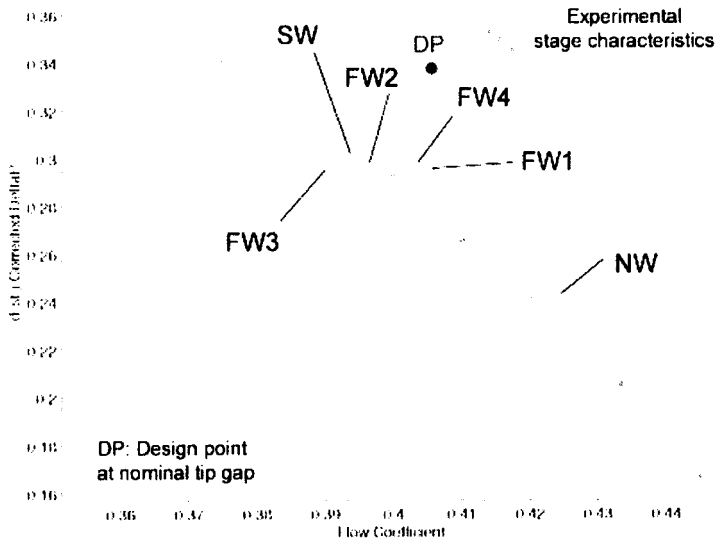

Figure 2-7: StageB Characteristic of E^3 with 3% tip gap from [21]. Our computation mean estimates are shown as circles (see Appendix A.1 for details)

comparable inlet flow conditions, so that any performance difference would reflect the impact of dynamic effects such as resonance between FW and TV. The mean operating points (see Appendix A.1) suggest that they appear to agree on the average.

Table 2.4 shows the principal flow parameters of each of the computed cases.

For information, the Reynolds number calculated in the rotor frame using the axial projection of chord as the length reference, is 4.5e5. SW is chosen as a baseline case for comparisons the FW cases with unsteady wakes in the stator frame. One may also note that performance comparison between SW and NW are not possible because operating points are very different

Parameters	NW	SW	FW1	FW2	FW3	FW4	RSNW
Flow Coefficient	0.424	0.394	0.405	0.396	0.39	0.404	-
PsPt coeff. Est.	0.244	0.302	0.298	0.298	0.299	0.298	-
Corrected DeltaP	0.3	0.282	0.312	0.284	0.272	0.309	-
Fluctuation Freq.(BP)	-	-	0.435	1	0.37	0.625	-
Fluct. freq(F_c^+)	-	-	0.69	1.584	0.586	0.99	-
$\frac{Pt_c}{Pt_b}$	1.099	1.1015	1.1012	1.0976	1.1036	1.103	-

Table 2.4: Mean flow parameters of all computed cases

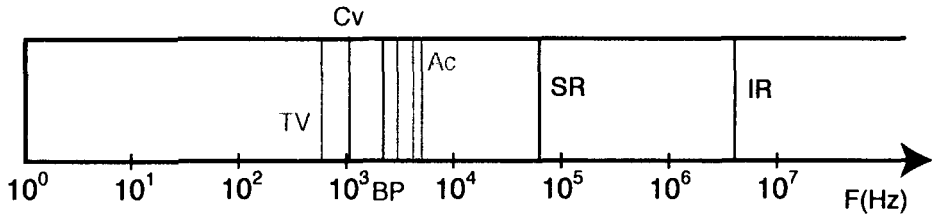

Figure 2-8: Comparison of the time scales involved in our computations

Timescale	Frequency	Period	Acronyms
Acoustic			
axial	2500 Hz	0.4 ms	Acx
circumferential(casing)	$> 3700Hz$	$< 0.27ms$	Acy
radial	2900 Hz	0.35 ms	Acz
Convective freq	1130 Hz	0.88	Cv
Blade Passing (wake from PS-¿SS)	2000 Hz	0.5 ms	BP
Rotation	2000 Hz	0.5 ms	Rot
Sampling rate	70.35 KHz	14.214 microsecs	SR
Time-stepping	3.87 MHz	0.2584 microsecs	IR

Table 2.5: Comparison of the main Timescales

due to the (or lack of) wakes. Our investigation on Wake-tip vortex interaction is thus centered around a spectral analysis of flow characteristics and blade excitation.

Time scales comparison

A summary of the typical timescales involved in our computations is shown in Table 2.5 . The acoustic time scales were estimated using the domain length of each dimension divided by the estimated average sound speed along this direction. The circumferential frequency is evaluated at casing (lower limit for the expected time period). All of them are graphically compared in Figure 2-8 . We note that the acoustic frequencies are significantly higher than the range of frequencies of interest - basically BP and lower - in our study. This is a guarantee that they will not interfere in our interpretation of the numerical results. One may also note the sampling rate and time-stepping several order of magnitude higher . Sampling errors are not likely to be an issue.

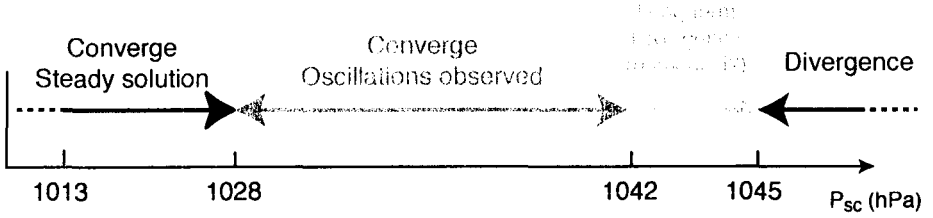

Figure 2-9: Numerical Convergence of the B-Rotor of E^3 with a 3% tip gap

Of note is the rotation timescale equal to BP scale due to our choice of equal blade count in IGV and Rotor time-step.

The operating point has been chosen so that the case with no incoming wake is near design but exhibits a large spontaneously unsteady tip flow. Observations from Vu [25] with UNSTREST on the same rotor geometry have been used as a basis to make this choice. He computed a range of different operating points and tip gaps with an unperturbed inlet flow and noted the presence and qualitative strength of self-induced unsteadiness in the tip flow region. A tip clearance of 3% span has been selected. This value also appeared to be the threshold minimal value beyond which the computed self-induced oscillation had a significant amplitude. For this clearance, numerous calculations, each corresponding to a different backpressure as shown in Figure 2-9 , This set of computations essentially cover a wide range of operating points, from high corrected mass flow (extreme left of Figure 2-9), to low corrected mass flow (extrame right of Figure 2-9 , stalling), and in each computed flowfield the tip vortex exhibits a self-induced unsteadiness.

The case with a flow coefficient of 0.424 (design value is 0.405 [21]) was chosen as baseline for unsteady computations. The flow coefficient is 0.424, as opposed to 0.405 at design point [21].

2.4.4 Wakes

A detailed description of boundary conditions implemented by UNSTREST can be found in J. Denton's manual for UNSTREST. Most of the work from our part on this topic has been devoted to implementing steady and unsteady incoming wakes.

In order to simulate wakes created by stator blades, a duct has been put upstream to the rotor, the end walls in the duct are fixed in the absolute frame. At the inlet boundary of this duct the wake is created at a fixed position, its properties changing with time if necessary. It is simulated by superposing a stagnation pressure defect over the baseline uniform boundary conditions. The fluctuation introduced in the wakes are additional defects that add up to the mean defect. The purpose is to have the same mean properties for all wakes -steady or unsteady. Figure 2-7 confirms that we have succeeded in having comparable time-average loading of the rotor stage.

It depends on an amplitude parameter A_d and a width parameter w is of the following form:

$$P_t = P_{unif}(1 - A_f P_c \exp(-(\frac{2 \cdot (y - y_c)}{w})^2) \tag{2.4}$$

where A_f is the main parameter that set the relative amplitude of defect. It has a monochromatic form:

$$A_f = 1 + P_{amp} \cdot \sin(2\pi \cdot \frac{t}{T_{fluct}}) \tag{2.5}$$

Hence, the shape of the wakes are set by 5 parameters:

$\mathbf{P_c}$ is the norm of the mean stagnation pressure defect

$\mathbf{y_c}$ is the circumferential position of the maximum defect, it remains constant with time.

$\mathbf{w}$ controls the width of the wake 2.4

$\mathbf{P_{amp}}$ is relative amplitude of fluctuation

$\mathbf{T_{fluct}}$ is the period of fluctuation

The values used for the generation of wakes in the various cases computed are given in Table 2.6 .

In the case of fluctuating wakes, the Pt defect has been chosen so that the maximum defect implies a zero velocity point (see eqn.2.4). Hence, the point of maximum defect simulate the position of the Trailing edge of the IGVs of the E^3 compressor.

This wake convects through the duct to the interface between the steady duct and the rotating grid of the rotor. The proper transmission of the wakes through this interface was

Parameters	NW	SW	FW1	FW2	FW3	FW4	RSNW
P_c	0	0.08	0.08	0.08	0.08	0.08	0
$y_c(m)$	0.045	0.045	0.045	0.045	0.045	0.045	0.045
w	0.005	0.005	0.005	0.005	0.005	0.005	0.005
P_{amp}	0	0	0.5	0.5	0.5	0.5	0
$T_{fluct}(sec)$	0	0	0.001148	0.0005	0.00135	0.0008	0

Table 2.6: Value of parameters for wake generation

an issue that has required modifications to the grid resolution and and to the mesh generation procedure in order to avoid an unwanted diffusion.

The upstream wakes are again represented by a symmetric two-dimensional Gaussian profile of stagnation pressure defect in the stator frame.

The velocity defect Δu induced by the stagnation pressure defect is parallel to the overall flow direction in the absolute frame. In other words, the velocity defect has no radial component.

2.5 Summary

The challenge of assessing the additional effects observed in a multi-stage axial compressor on the blade forced response of a rotor or stator due the blade-row interaction has been assessed. The difficulty of approaching the complex problem of inter-blade-row interactions using numerical simulations has lead us to only consider a group of stator-rotor-stator as a module of the entire system. The purpose is to simulate and analyse the interactions within the group and evaluate from the computed results how they could be extrapolated to a multistage environment. The blade forced response in a stator have been studied in two situations: the stator is subjected to a steady wake or and an unsteady wake in the rotor frame. The assessment of the blade forced response in a rotor may require that sources of unsteadiness, internal to the rotor, be accounted for. Thus, three situations have been computed: (1) a rotor is subjected to a uniform inlet flow so that inherent source of excitation can be assessed, (2) a rotor is subjected to a steady or unsteady wakes in the stator frame, (3) a rotor-stator group is subjected a uniform inlet flow, so that the effect of the pressure field disturbance induced by the downstream stator on the rotor blade excitation could be quantified. Different codes have been used for the rotor and stator computations, their respective characteristics have been described. In all cases, the

steady or unsteady incoming wakes have been simulated. The unsteady computations have been carried out with a single passage per blade row.

Chapter 3

Unsteady Flow Computations in a Stator Stage

3.1 Introduction

In this chapter, computed results by Valkov [22, 23] on the interaction of upstream rotor wakes with stator will be used to assess the characteristics of unsteady pressure fluctuations on the stator blades. As noted in Chapter 2, two situations will be considered and analyzed here: (1) (steady) rotor wakes are assumed to be steady in the rotor frame and (2) (unsteady) rotor wakes are considered to be unsteady in the rotor frame. The wakes interact with a midspan section of the stator on a two-dimensional basis.

This chapter will be organized as follows. We first present computed results for (1) and the associated computed response of pressure distribution on stator blades. This is then followed by presenting the computed results for (2) together with the associated computed response of pressure distribution on stator blades. The results are used to answer the following question: What is the validity of assuming the rotor wakes to be steady in rotor frame when one is examining the unsteady response of pressure distribution on the stator blades?

3.2 Steady Rotor Wake-Stator Blade Interaction

This section examines the unsteady flow arising from the two-dimensional interaction of upstream wakes with a midspan section of the stator (see Chapter 2). The aim is to assess the

effects by which wakes influence the unsteady static pressure distribution on stator blade surface and the responsible flow processes. The computations were carried out by Valkov [23] at a design flow coefficient of 0.45, Reynolds number of 247,000.

The disturbance flow can be described in terms of disturbance vorticity $\Delta\Omega$, defined as the difference in vorticity between the unsteady flow and the steady flow. Instantaneous disturbance vorticity field is shown in Figure 3-1 for baseline 25% wakes. The wakes are essentially transported in the manner put forth by Smith (1966). Individual wake segments are stretched. Their suction surface (SS) and pressure surface (PS) end travel at different speed, and leave the stator with a shift relative to the other wakes. The stronger wakes are characterized by a more pronounced migration. Figure 3-1 also shows vortex shedding from the trailing edge and non-transitional vortical disturbances in the boundary layer; the suction side boundary layer disturbances (referred to as BLDs) could also be an indirect source of unsteadiness. The BLDs seen in wake interaction calculations have a characteristic structure. Each BLD originates on the leading edge at the moment of wake interception. It is composed of two thin regions of high negative and positive shear respectively. These regions are lifted away from the suction surface by the wake, and are convected along the edge of the boundary layer. Computational experiments reported in Valkov and Tan (1996) show that these vortical disturbances originate from displacement of the boundary layer vortex filaments under the suction effect of the wakes while those on pressure surface is a result of wake jet directed toward it. A simplified model based on distortion of boundary layer vortex could describe the balance between transport of disturbance vorticity $\Delta\Omega$, and production from convective redistribution of steady flow boundary layer fluid under the effect of a transverse velocity disturbance ΔV_n. The model helps explain why (a) BLDs are primarily produced in the boundary layer/bulk flow interface over the foremost part of the blade, (b) the primary BLDs contain negative disturbance vorticity. We next proceed to examine the change in unsteady static pressure distribution on the stator blade surface.

Shown in Figure 3-2 (a) is a contour of pressure disturbance distribution on the stator blade surface spanning over a finite time interval. Indicated on the figure are locations of leading edge and trailing edge on the abscissa that denotes distance along the blade surface. The vertical axis denotes time in unit of 0.0005 convective time (i.e. flow through time from blade leading edge to trailing edge) through the stator blade passage. Figure 3-2 (b) displays the computed results of Figure 3-2 (a) in three-dimensional perspective with the vertical axis denoting the

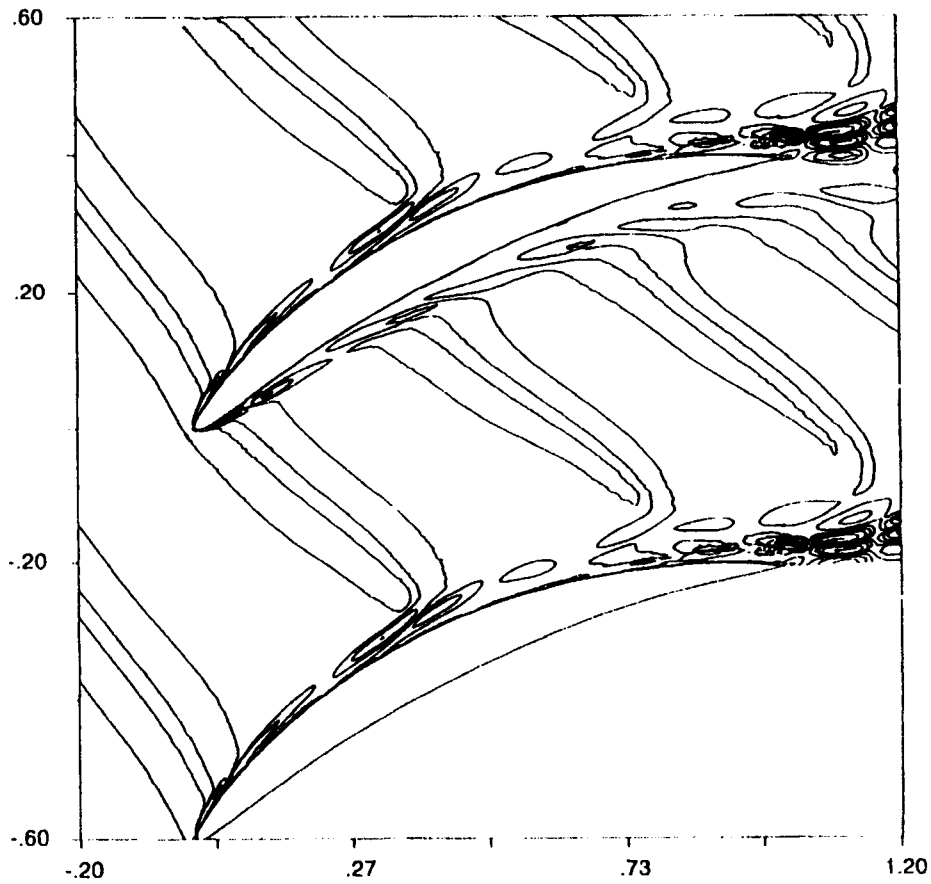

Figure 3-1: Contour of Disturbance Vorticity Distribution Associated With The Interaction Of Stator With Upstream Wakes (Assumed Steady In Rotor Frame) Moving In The Tangential Direction [Valkov]; The Arrow Indicates The Direction Of The Disturbance Velocity From Suction Side To Pressure Side Within The Wake; The Vortical Disturbances In The Vicinity Of Suction And Pressure Surface Are A Result Of Wake-Boundary Interactions

static pressure disturbance magnitude and with time on one horizontal axis and distance along blade surface on the other. The regions corresponding to high and low pressure disturbance can be corroborated with the disturbance flow of Figure 3-1 . A second harmonic, probably due to nonlinear effects, is noticeable on the pressure side as indicated in Figure 3-2 (a) and (b). The blade surface frequency spectrum distribution of the pressure disturbance is shown in Figure 3-2 (c). As to be expected for wake steady in the rotor frame, the frequencies higher than the fundamental blade passing show a decaying pattern. However this is not so in the situation when the wakes are unsteady (i.e. fluctuating in time) in the frame of the rotor.

3.3 Unsteady Rotor Wake-Stator Blade Interaction: Effects of Unsteady Fluctuations Within Wakes

Experimental data shows temporal fluctuations of velocity within compressor wakes. These fluctuations may be a substantial fraction of the wake velocity defect. Thus a set of computations by Valkov [23] have been used to assess the role of such fluctuations on rotor wakes-stator interaction and on unsteady pressure distribution on stator blade surface. As noted in Chapter 2, the wakes used for this purpose have the same 'ensemble-averaged' profile and properties. For each wake, the defect is sinusoidally varied in time with an amplitude equal to the ensemble-averaged value, and with a time period T_i ranging from 1/7 to 2.0 times the blade passing period T_p. The choice of amplitude is representative of fluctuations seen near the rotor trailing edge (Brookfield and Waitz, 1996). The ratio T_i/T_p takes fractional values ensuring that a fixed point on the blade does not experience the same disturbance at every interaction. Small T_i/T_p ratios (1/7-3/7) constitute a simplified representation of measured wake fluctuations (Kotidis and Epstein, 1991; Brookfield and Waitz, 1996) while large ratios (4/3-2) are used to bound the time scale.

Figure 3-3 (a) illustrates the typical vortical structure of the unsteady flow field for T_i/T_p (wake fluctuation timescale/interaction timescale) with value of 0.4. Thus T_i/T_p influences the dynamics of the wake during its transport through the stator. Computed results (not shown here but reference should be made to [23]) indicate the existence of three distinct regimes: low-frequency ($T_i/T_p \geqslant 1.3$) intermediate-frequency ($0.2 \leqslant T_i/T_p \leqslant 1.3$) and high frequency ($T_i/T_p \leqslant 0.2$) fluctuations. For high-frequency fluctuations, the individual vortices comprising

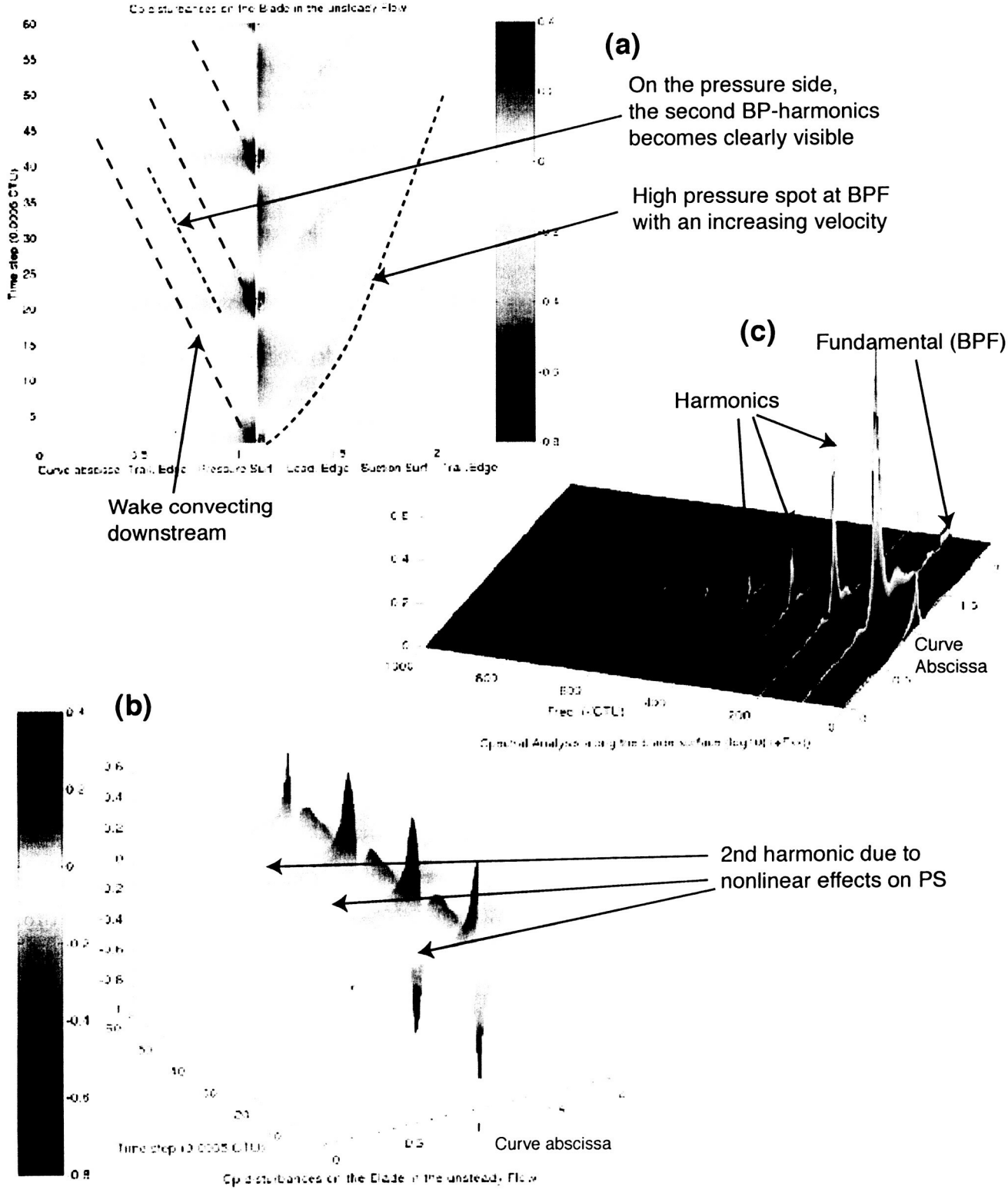

Figure 3-2: A Representative Result Associated With The Interaction Of A Stator With Upstream Moving Wakes Assumed Steady In Rotor Frame

the wake appear to coalesce into a steady wake, transported through the stator in the same manner described above. For low-frequency fluctuations, the lengthscale over which wake properties vary is larger than the blade-to-blade spacing, and the individual wake segments are also transported as described above ((Figure 3-1). For intermediate frequencies however, the wake fluid forms passage vortices that persist far downstream (Figure 3-3 a). Boundary layer disturbances (BLDs), similar to those seen with ensemble-averaged wakes, are present over the suction surface for all frequencies.

The disturbance vorticity distribution corresponding to interaction of the stator with upstream rotor wakes that fluctuate at a frequency one third the blade passing frequency is shown in Figure 3-3 (a). As such there is an additional time scale in addition to that associated with blade passing. The disturbance vorticity pattern in Figure 3-3 (a) is very different from that in Figure 3-1 . Likewise the corresponding static pressure disturbance distribution shown in Figure 3-3 (b) is different from that of interaction with steady wakes shown in Figure 3-2 (a). The frequency spectrum distribution of the pressure disturbance shown in Figure 3-3 (c) indicates that amplitude of pressure disturbances corresponding to frequencies that are 4/3,7/3, and 10/3 times the blade passing frequency are unexpectedly amplified. This has the implication that the width of the frequency spectrum is enlarged by the interactions so that increased excitation of higher (blade) modes can be expected. It is tentatively hypothesized that the amplification could be a result of the interactions of fluctuating wake disturbances with those associated with blade passing events. Since the fluctuation frequency is connected to the blade passing frequency of the upstream rotor, the observed amplification and hypothesized interactions can effectively lead to the persistence/presence of excitation associated with upstream wakes many blade rows downstream. Post processed results in [23] on interaction of ensemble-average rotor tip vortex and secondary vortex show response (as measured in terms of unsteady static pressure disturbance changes) similar to that of stator interacting with two-dimensional rotor wakes. While no computations involving fluctuating tip vortex in rotor frame has been simulated, one may infer that if the tip vortex is taken to be unsteady in the rotor frame the response in the downstream tip region can be expected to be similar to the case of stator interacting with upstream fluctuating rotor wakes.

(a) contour of disturbance vorticity in unit of ratio of mean velocity to blade chord

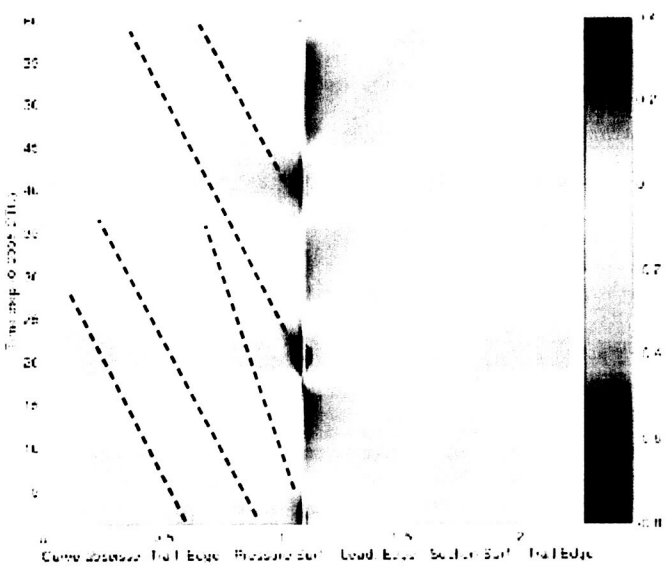

(b) Blade surface Static pressure (Cp) disturbance distribution over a finite interval of unsteady wake blade interaction

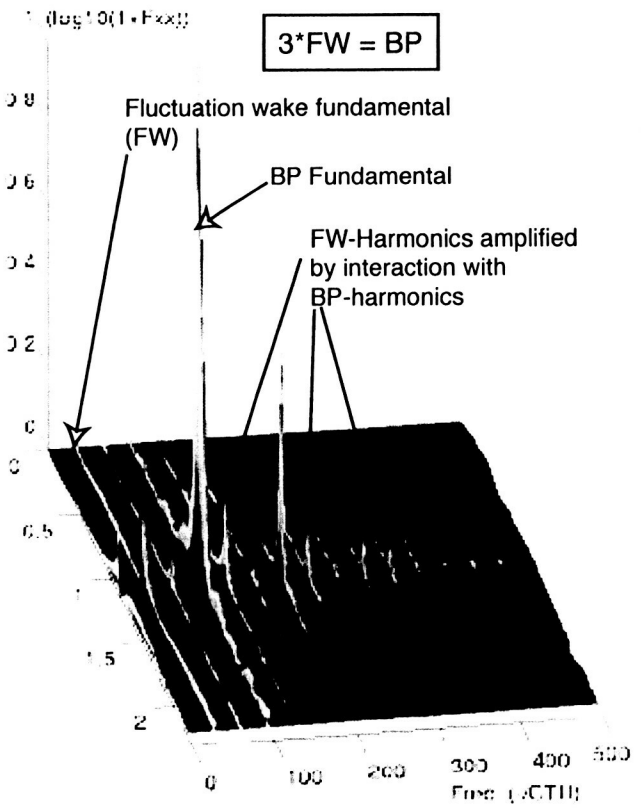

(c) Blade surface spectrum distribution of pressure disturbance

Figure 3-3: Unsteady pressure disturbance and corresponding frequency spectrum on blade surface associated with disturbance flow field due to interaction of stator blade with upstream moving wakes that are fluctuating with time in the rotor frame

3.3.1 Summary

The dynamic effects of steady and unsteady wakes on a stator blade excitation and the flow mechanisms induced by the interaction of wakes with boundary layers have been described and analyzed. When steady wakes in the rotor frame are input into the stator row, it is found that the spectrum of the pressure distribution disturbance on the blade surface contains the Blade passing frequency and its harmonics, with a decaying amplitude as the frequencies increases. However, in the case of unsteady wakes in the rotor frame, the spectrum of blade excitation exhibits unexpectedly amplified higher frequencies. Besides the main fundamentals corresponding to the blade passing frequency and the frequency of excitation of the incoming wakes, modulations of the former excitations are observed at higher frequencies with an amplitude several order of magnitude higher than that of the harmonics of the excitation computed separately. The present choice of the distinct frequencies of the two excitation sources has proven to further amplify this effect. This has important implication on the prediction of frequency content of blade forced response in a multistage compressor, as this suggests that under certain conditions the spectrum of incoming disturbances is enriched by its interaction with a stator stage and unexpectedly high frequencies might persist many blade rows downstream with potential unpredicted aeromechanical consequence.

Chapter 4

Unsteady Flow Computations in a Rotor Stage

In this chapter, the results of unsteady flow computations in a rotor stage are discussed. In the first section, the tip vortex flow instability is characterized in a computation with uniform inlet flow. Its impact on the blade pressure distribution is also assessed. The interaction of incoming wakes with the inherently unsteady tip vortex flow is then analyzed with a particular emphasis on the way the frequencies interact in the power spectrum of the blade excitation and rotor wakes. The effect of the frequency of fluctuation of incoming wakes on the blade forced response is assessed in a third section. The frequency is adjusted to match the TVF and resonance effects are addressed.

4.1 Self-induced tip vortex response

This section presents the results obtained from the computation of a rotor blade row with a 3% tip gap subjected to a steady inlet flow.

4.1.1 Characterization of a spontaneous unsteadiness in tip flow region

Figure 4-1 shows a very high-resolution (made from 140,000 time steps at sampling rate of 3.87Mhz) Fourier Transform of the total mass flow through the stage in the baseline case. The power spectrum is shown on the y-axis, the x-coordinate shows the frequency divided by the BP frequency. A clear peak appears at 0.45 +/-0.01 BPF. Here, this frequency will be denoted

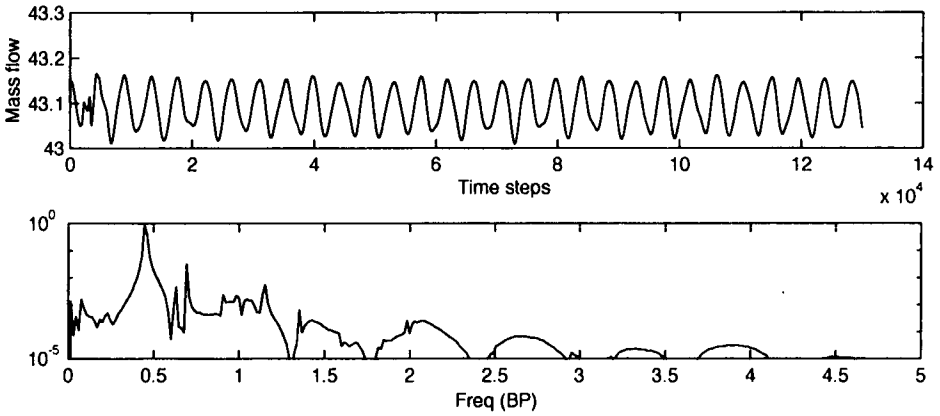

Figure 4-1: Accurate Spectral Analysis of Mass Flow

by the acronym TVF (Tip Vortex Frequency). The variation of mass flow do not exceed 0.3%. There appear to be no relationship between TVF and BPF. Often, the reduced frequency:

$$F_c^+ = \frac{TVF \cdot C_x}{U_{x,inf}} \tag{4.1}$$

is used to characterize the tip vortex fluctuation; it is the product of TVF and the time it takes for a particle to traverse from the inlet plane to the exit plane. For the present computed flow field, the value is 0.69.

Recent work by Mailach [13] and Bae [1] provides time-resolved data taken in two different low-speed compressor cascades, the former on the Dresden LSRC compressor, the later on E3 stage B linear cascade. Pressure measurements [13] and hot wire measurements [1] were carried out in the tip region, and a tip vortex instability similar to that observed in the computed flow field here was observed. Although the dimensional frequencies are both of different order of magnitude, the data in both experiment setups show a characteristic reduced frequency F_c^+ of 0.65 to 0.7, which is in accord with our numerical result of 0.69.

While the tip vortex flow is confined to the rotor tip region, the effect associated with its unsteadiness (i.e. tip vortex fluctuation) is observed to permeate throughout the blade passage. Time-resolved computation of space-integrated (ie. area-averaged) value such as that of blockage or rotor loss coefficient showed that this is the case.

Figure 4-2 and Figure 4-3 show computed temporal evolution of tip leakage mass flow,

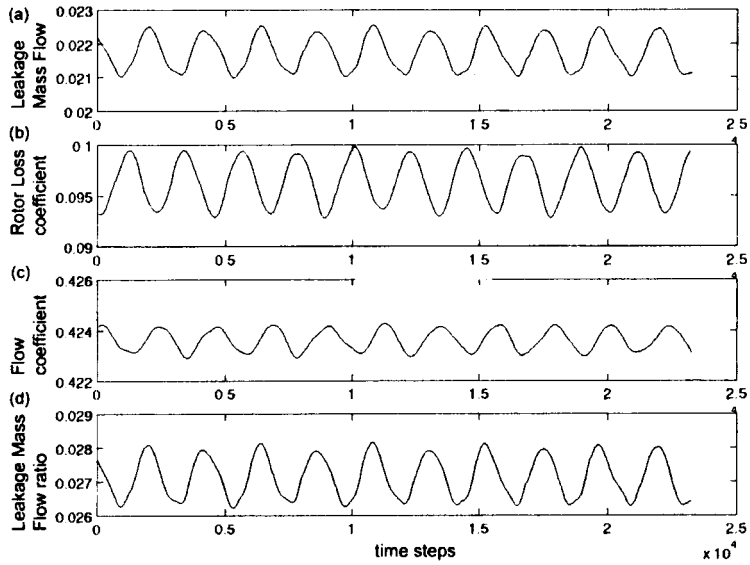

Figure 4-2: Evolution of (a) Tip leakage mass flow (b) Rotor Loss Coeff. (c) Flow coefficient and (d) Leakage/total mass flow ratio

tip mass flow ratio, mass-averaged rotor loss coefficient and flow coefficient as well as their associated spectrum. The first set of data (Figure 4-2 (a)) shows the evolution of the leakage mass flow through the tip gap. Figure 4-2 (b) shows the mass-averaged loss coefficient, defined as:

$$\bar{\omega} = \frac{\bar{P_{Tb}} - \bar{P_{Tc}}}{\bar{P_{Tb}} - \bar{P_b}} \tag{4.2}$$

where $\overline{(\ )}$ denotes mass averaging over an axial cut, P_{Tb} is the stagnation pressure at inlet, P_{Tc} the stagnation pressure at exit and P_b the static pressure at inlet. Figure 4-2 (c) shows the time variation in flow coefficient $\frac{U_{x,inf}}{U_{tip}}$, where $U_{x,inf}$ and U_{tip} denote upstream time-mean axial velocity in the core inlet flow and the tip rotation velocity respectively. And Figure 4-2 (d) shows the time variation of the tip gap mass flow normalized by the total mass flow through the passage.

As one can deduce from Figure 4-3 , all have a clear overwhelming oscillation equal to 0.45 BP. We also note that this peak is embedded in a broad low frequency band. This is in accord with the broad band in the experimental surveys of 'Rotating Instabilities' (RIs) by Mailach.

The following observations confirm that this oscillation is closely related to the tip region flow:

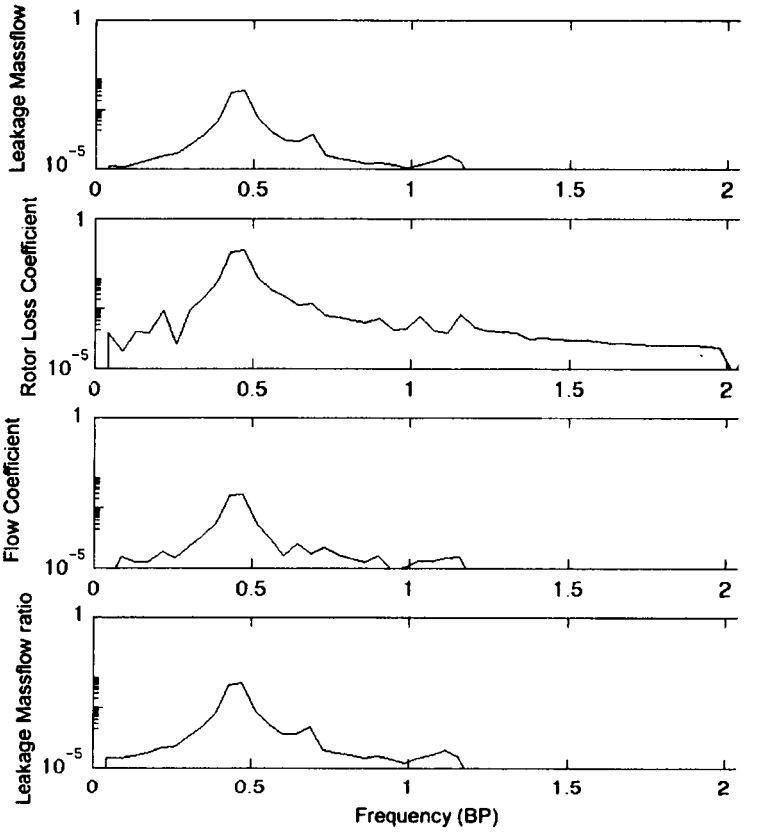

Figure 4-3: Spectral analysis corresponding to Figure 4-2 . (a,b,c,d) are frequency content corresponding to Figure 4-2 (a,b,c,d)

- The variation of the tip gap mass flow is as high as 6.8%,while the total inlet mass flow varies only by 0.3%. This results in a 6.7% variation of the tip mass flow ratio suggesting that this spontaneous oscillation mainly pertains to the tip region.
- The flow coefficient shows only small variations of 0.3%.

It can thus be inferred that the effects of tip flow instability in a rotor subjected to uniform inlet flow, are of engineering interest to warrant further interrogation of its characteristics.

4.1.2 Frequency and Structural Content of Tip Flow Region

So far, we have had an overall look at the unsteady behavior of the rotor. We have noted that the tip flow region appears to be where this observed self-excited oscillation is. In this subsection, our objective is to characterize the observed/computed tip vortex unsteadiness and determine its evolution through the passage.

Development of Tip Vortex

The tip vortex at the early stage of its development (close to the inlet plane of the passage) can be observed to be oscillating from examining the radial velocity contour plots. The tip vortex core and its unsteady motions can be located.

Figure 4-4 shows snapshots of the core of vortex taken every quarter of TVP period. The tip vortex core appear to oscillate at a frequency higher than TVF. A pressure probe, denoted as **Probe 1**, was placed inside the core. The measurements, shown in Figure 4-5 , confirm that two frequencies (and their modulations) are observable in the core of the tip vortex. The new frequency corresponds to the motion of the tip vortex core; it is denoted by LVCF. It appears to have no relation to TVF or any of its harmonics. LVCF is approximately 1.15 BPF.

Another pressure probe, denoted as **Probe 2** was placed outside of the tip vortex core, but still in the tip flow region. It shows (see Figure 4-6) that LVCF has a much lower amplitude compared to TVF and consequently modulations of TVF and LVCF (for instance LVCF-TVF) are more than two order of magnitude lower than the dominant harmonics of TVF. It confirms that LVCF is a frequency only observed in the immediate vicinity of tip vortex core.

In any case, even at the center of the TV core, TVF remains the dominant frequency

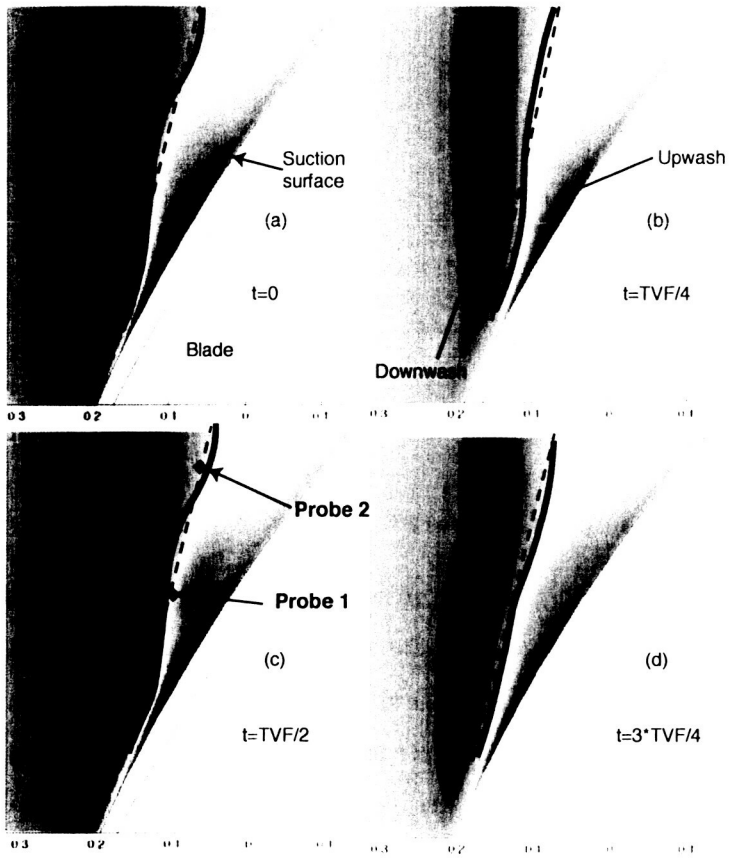

Figure 4-4: Relative Radial velocity around the tip vortex at 95% span and t=0, t=TVP/4, t=TVP/2, t=3TVP/4 with TVP the TV period. The dashed line is a reference line, the bold curves depicts the position of the tip vortex center

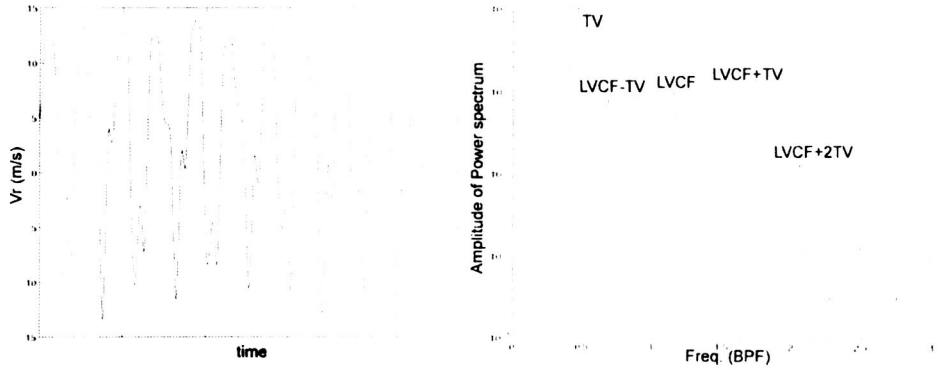

Figure 4-5: Computed Static pressure indicated at Probe 1, 25% C_x and 15% pitch

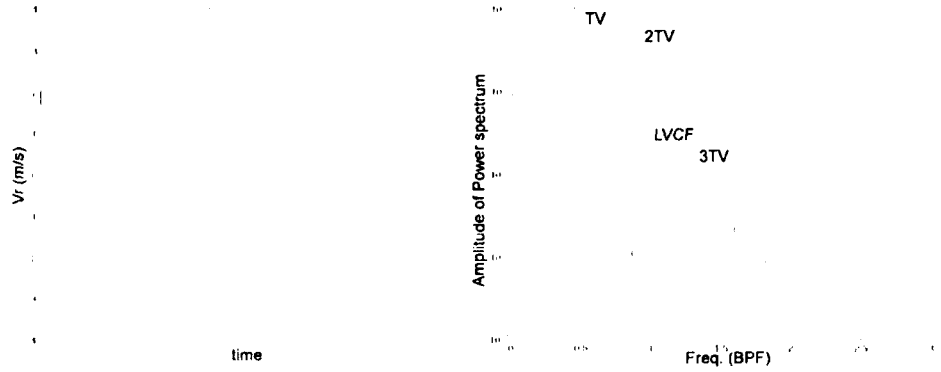

Figure 4-6: Computed Static pressure indicated at Probe 2, 52% C_x and 31% pitch

Dominant Frequency in Tip Vortex

Computed time variation of static pressure at 32% pitch and 95% span confirms the large pressure variations in the region where the tip flow has developped, this is shown in Figure 4-7 . In this figure, a series of pressure probes from 20% to 100% C_x as well as their power spectrum are shown. The power spectrum have the squared amplitude of spectral components of the signal as ordinate. The abscissa are expressed in fraction of the TVF. On the left hand part of the figure, a logarithm graph summarizes the evolution of the two first TVF harmonics.

In the front part of the tip flow (20-30% C_x), a variety of peaks of comparable amplitude cover the power spectrum. These peaks are TVF and LVCF harmonics as well as some of their modulations.

As we proceed downstream, LVCF disappear from the power spectra at a location corresponding to 40% axial chord. From that position onward, only TVF and its harmonics persists. For the computed results shown in Figure 4-7 (ii), the amplitude of pressure fluctuation appears to be the largest in the mid-chord region. However, similar results for pitch position near to the blade pressure surface indicate that the amplitude of pressure fluctuation increases monotonically in the downstream direction.

Figure 4-7 elucidates several points:

- the presence of an oscillation at TVF frequency is clearly linked to the tip flow.
- TVF is clearly omnipresent in the tip region while LVCF is only a local and secondary excitation.

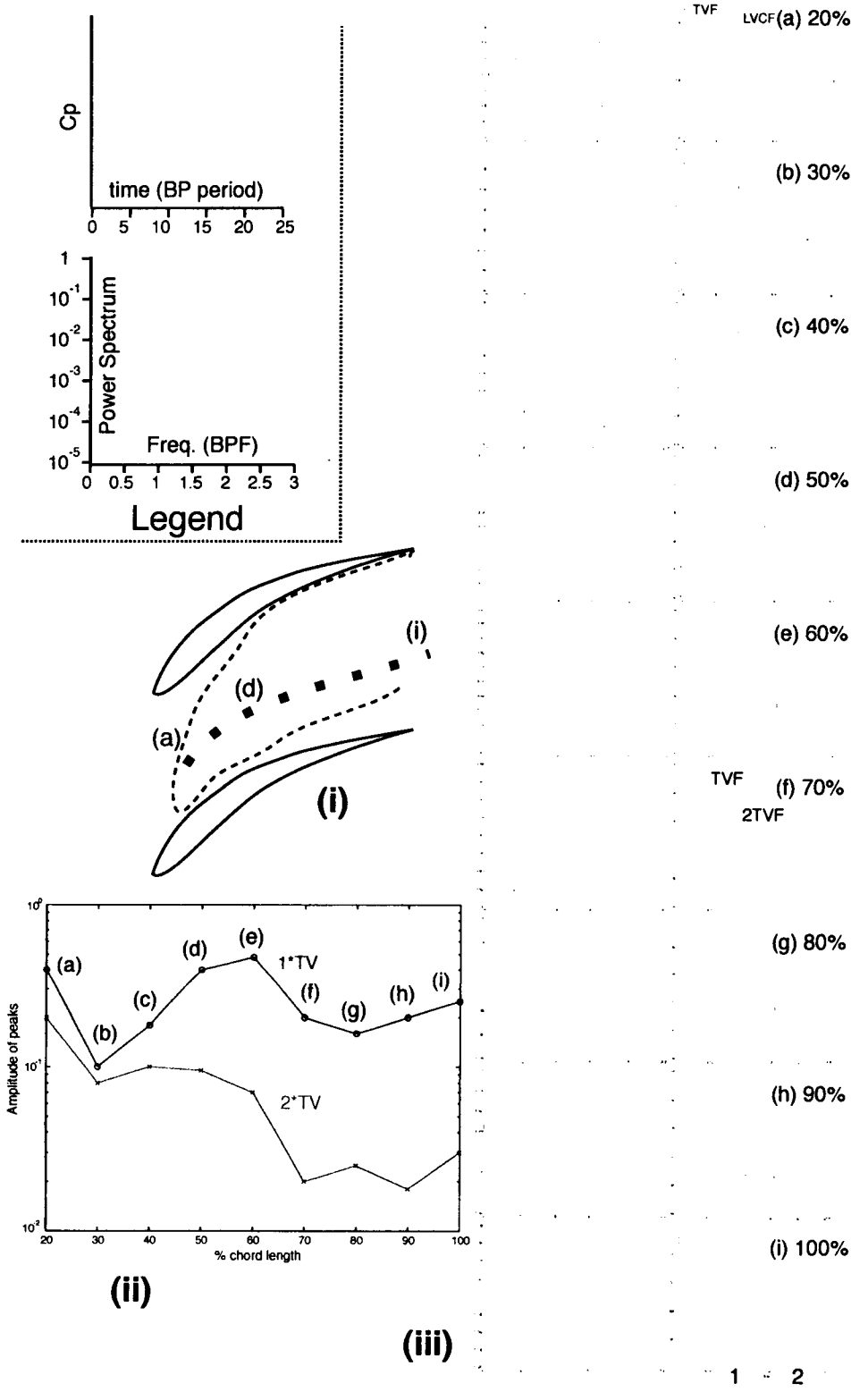

Figure 4-7: Series of static pressure probes and their corresponding power spectrum in the tip flow region. 95% hub-tip positions and 32% pitch

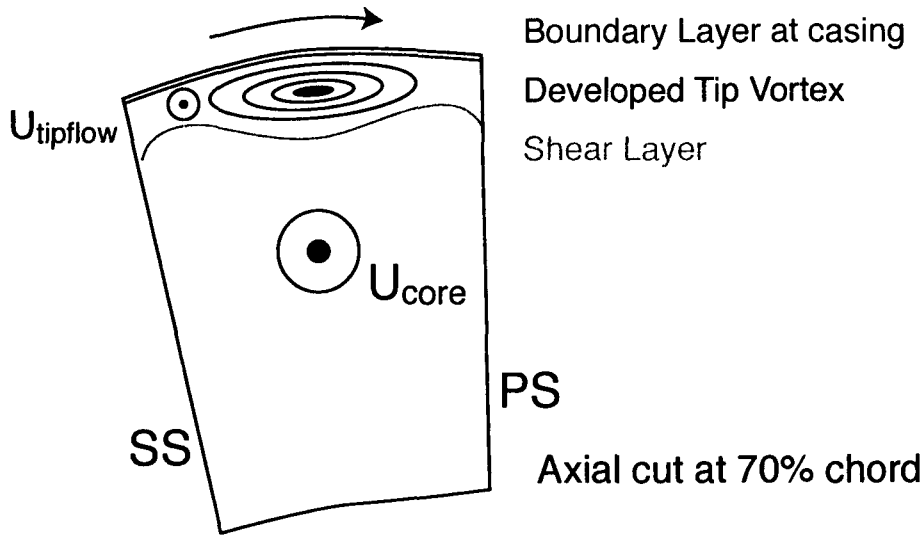

Figure 4-8: Typical axial cut of tip flow region

- The amplitude of TVF increases as we proceed downstream.

Structural Content of Low-Momentum Tip Region

Following the previous observations, several questions can be posed:

- Is there some flow pattern which propagates downstream that would explain the dominance of TVF at all chord position in the tip flow region?
- Why is LVCF only locally observable in the tip flow up to 40% chord?
- What is the evolution of the extent of the low-momentum tip region with time and axial chord?

These questions have led us to interrogate the structure of the low-momentum tip region.

The interaction of the tip clearance flow with the core flow creates a region of low-momentum flow near the casing. The interface separating this region from the core flow is hence a zone of high shear as sketched in Figure 4-8 . Observations and the computation of animated pictures of entropy contour graphs have shown that the interface is not steady in the rotor frame, its distance to the casing locally fluctuates as shown in Figure 4-9 . Figure 4-9 shows a contour plot of entropy on a plane at 80% pitch, and one on an axial plane at 70% C_x.

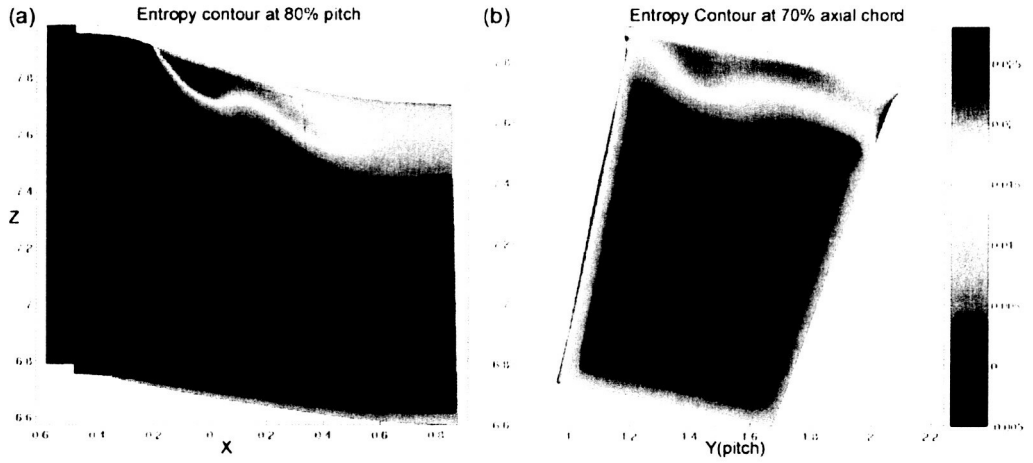

Figure 4-9: Left: Entropy contour showing TV pulsations in a 80% pitch cut; Right: Entropy contour in a 70% Cx Axial cut

The pattern of variation in the interface bounding the low momentum region corresponds to that of a wave-like behavior as it propagates downstream. This wave-like pattern of the tip flow region was observed to have a flow structure, as indicated in Figure 4-10 , that is observed orthogonal to the direction of the core velocity direction of the core flow. Mailach [13] measured pressure patterns (probably associated with the flow structure computed here propagating downstream). As will be shown in the next section, such pressure pattern was observed in our computed results and found to correspond to the pattern of wave-like interface bounding the low-momentum region.

The present set of computed results indicates that the tip vortex structure is not identifiable beyond approximately 40% C_x. Beyond that point, the tip flow region is just a region of low momentum flow, no vortex core can be identified anymore (see Figure 4-9 (b)). This explains why LVCF is only observable locally in the flow region within the first 30% C_x. It was shown that its presence was related to the tip vortex core motion. Its disappearance in the frequency spectra beyond 40% C_x may be associated with the observation that beyond this location, there is no distinct tip vortical structure. Instead discrete patterns of high entropy are formed beyond 40-50% chord corresponding to the zones of tip clearance flow (which is observed to vary spatially and temporally).

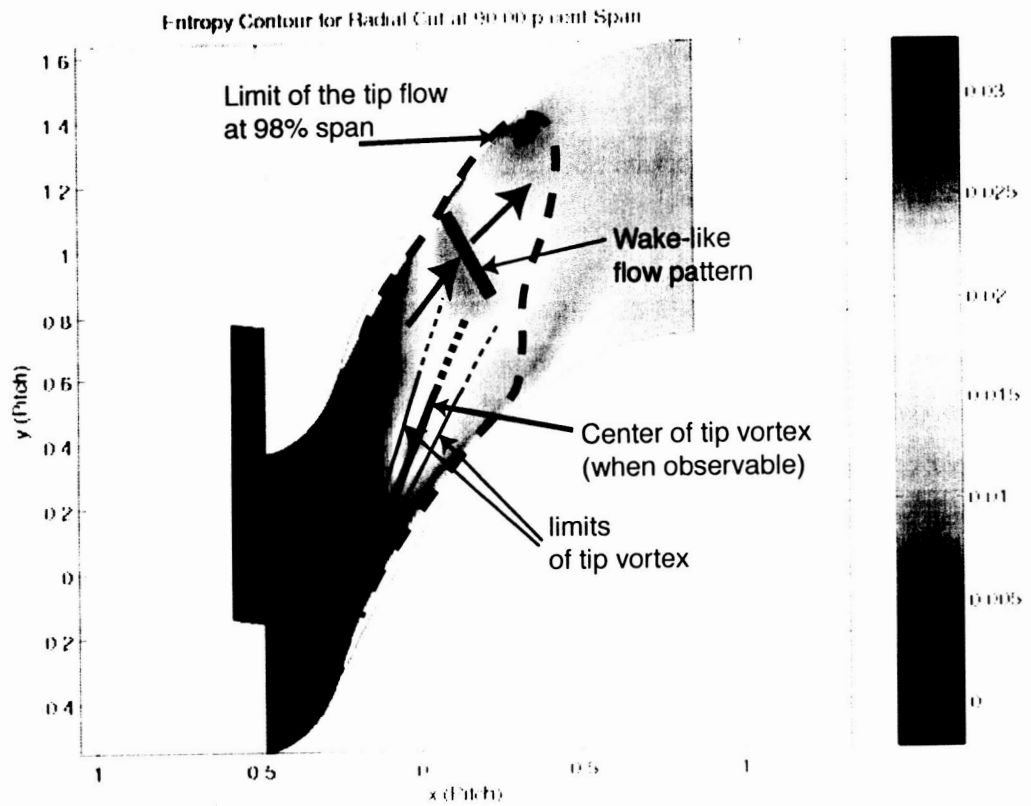

Figure 4-10: Entropy (normalized by specific heat at constant pressure) contour at 90% span

Based on our observation of the structural aspect of the tip flow region, a systematic method of computation was needed in order to reliably characterize the extent of the low-momentum region as a function of time and axial chord. By definition (see [11]), calculating the blockage on an axial cut plane is in fact calculating the ratio of the effective surface of low-momentum over the cross section surface on the axial cut plane. Hence, we have the method of computation of the tip and total blockage defined by Khalid [11] were implemented, and contour plots of the blockage as a function of time and axial position were produced.

It is important here to note that blockage computations in this paper are not aimed at assessing the performance of the rotor in any way, but rather at reliably determining the effective extent of the low-momentum flow region.

The plots for the NW case are shown in Figure 4-17 and discussed in detail in the next section. It is found that wave-like pattern of blockage variation move through the blade row at a frequency of TVF and with a axial velocity equal to 0.42 times the axial core throughflow velocity $U_{x,inf}$. This velocity is lower in the first 30% C_x at 0.28 $U_{x,inf}$. The use of blockage provides us with another alternative to discern the propagating wave-like pattern of tip flow region in an indirect manner and to estimate its velocity of propagation through the rotor blade row. This changing velocity is equal to the ratio of the cosine of the flow angle at inlet and exit of the rotor, which confirms again that the motion of the wave-like pattern is directly linked to the (changing) direction of the velocity of the core flow.

4.1.3 Origin of TVF

Bae [1] hypothesized that the tip vortex unsteadiness could be explained by Crow instability model. Crow presented an inviscid model of a pair of parallel counter-rotating vortices, which under certain conditions exhibit flow instability. Bae suggested that the tip vortex, together with its image with respect to the casing endwall, approximate a pair of counter-rotating vortex and would thus develop a self-induced instability analogous to Crow type of instability. Bae compared his measured TVF frequency with Crow's predicted frequency and they were in agreement within a 20% error margin.

However, in light of the computed results presented so far, we showed the following points:

- The tip vortex - when observable at 10-40% chord - exhibits a LVCF frequency of motion

different from TVF.

- wave-like pattern of the interface separating the core flow from the low momentum tip flow region persists and amplifies even when the tip vortex core is no longer identifiable

- TVF is observable throughout the tip region, it is dominant even near the tip vortex core (20-30% chord). LVCF induced by the tip vortex motion at that position coexists with TVF.

The above observations tend to imply that the tip vortex motions do not seem to drive the TVF fluctuation measured in the entire tip region flow. Thus Bae hypothesis cannot be conclusively inferred from the computed results here.

Still, it is thought that TVF is related to the dominant tip region instability, and the present computed results cannot conclusively demonstrate that the tip vortex core structure (as opposed to a region of low momentum flow) is a cause of this unsteady phenomenon.

In the next subsections, the implications of the self-excited oscillation in the tip flow region are examined.

4.1.4 Impact on Blade Surface Pressure Distribution

The unsteady flow behavior associated with the tip clearance in a rotor subjected to uniform inlet flow has been delineated. It is now appropriate to address its implication on blade excitation. Figure 4-11 show Cp profiles at three spanwise positions on the blade surface: 10, 60, 99% span at a given instant. The Cp profile at 99% span is different from nominal Cp distribution at midspan. The lower pressure region corresponding to about 40% chord on the SS was to be expected if we consider the high velocity of the tip clearance flow. However, the lower pressure region on the PS is usually not observable in steady rotor computations. The cause of this lower pressure is the unsteady component of the static pressure on the blade surface near the tip, as shown in Figure 4-12 .

Of note is the definition of the pressure coefficients in this thesis; it is measured in term of dynamic head based on the axial velocity U_x:

$$Cp = \frac{p - p_{inf}}{0.5 \cdot \rho_{inf} \cdot U^2_{x,inf}} \tag{4.3}$$

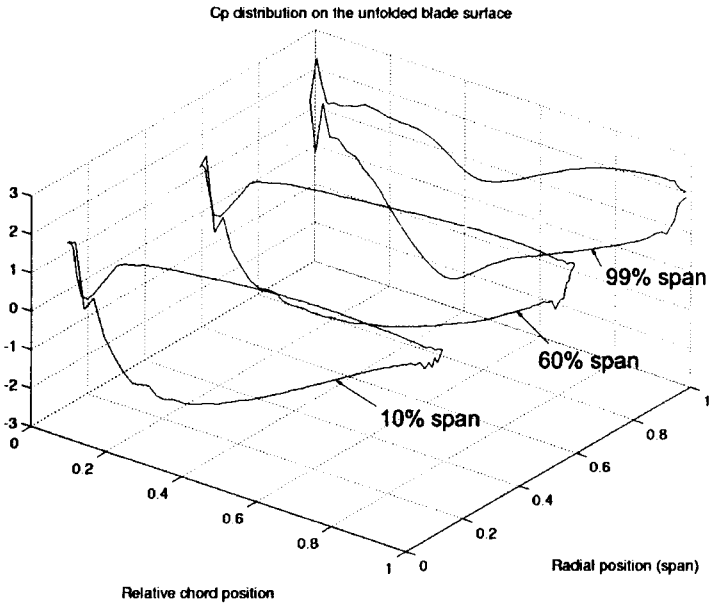

Figure 4-11: Cp profiles at different span sections on the blade surface at a given instant

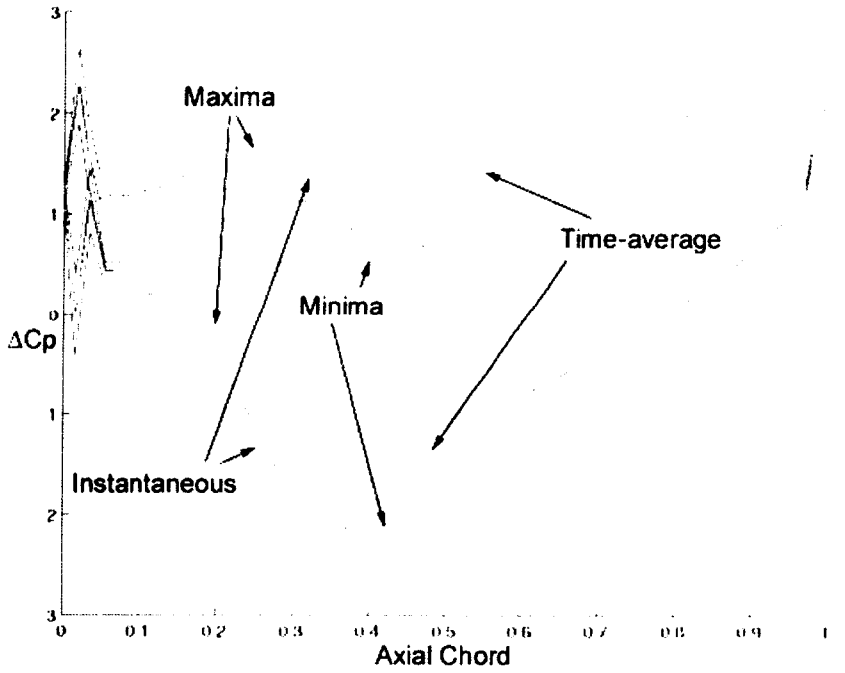

Figure 4-12: Time Analysis of Cp profiles on the rotor blade section at 99% span. Minimum, Mean and Maximum Cp profiles are shown. A profile at a given instant is also represented.

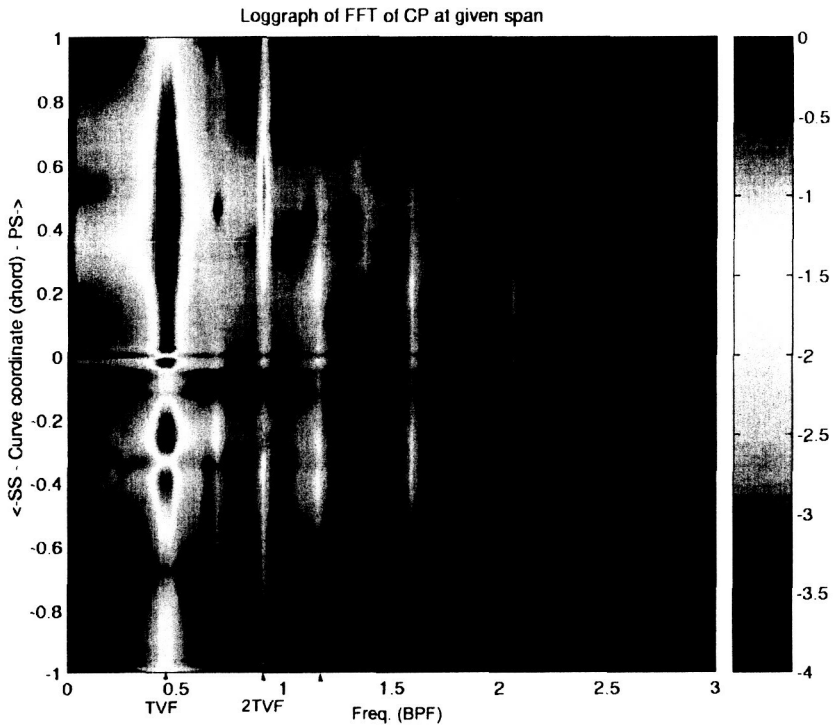

Figure 4-13: Power Spectrum of Cp on PS and SS at 99% span on blade surface

The time-averaged Cp profiles and the locus of the local minima and maxima of Cp are shown in Figure 4-12 . The variations of Cp with time are much greater on the PS than on the SS. They are as high as 30% of the local Cp value on the PS, with a maximum variation at about 40% chord, and it is less than 10% on the SS. The time-average Cp distribution on the SS indeed shows that the low pressure spot is due to the presence of the tip clearance flow and is located at fixed position about 35% chord.

In contrast, on the PS, the snapshot shown on Figure 4-12 indicates that the extrema are not reached at the same moment, but regions of lower and higher pressure propagates downstream at $0.42 \cdot U_{x,inf}$ in accord with the velocity of the wave-like pattern described in the previous section.

The spectrum of the pressure probe on the PS and SS at 99% span on the blade surface have been computed as shown in Figure 4-13 . The ordinate is the axial position in terms of chord length. It is negative for the SS, positive for the PS. Hence, 0 indicates the leading edge, 1 or -1 indicate the trailing edge. It can be noted that the TVF is again the dominant frequency

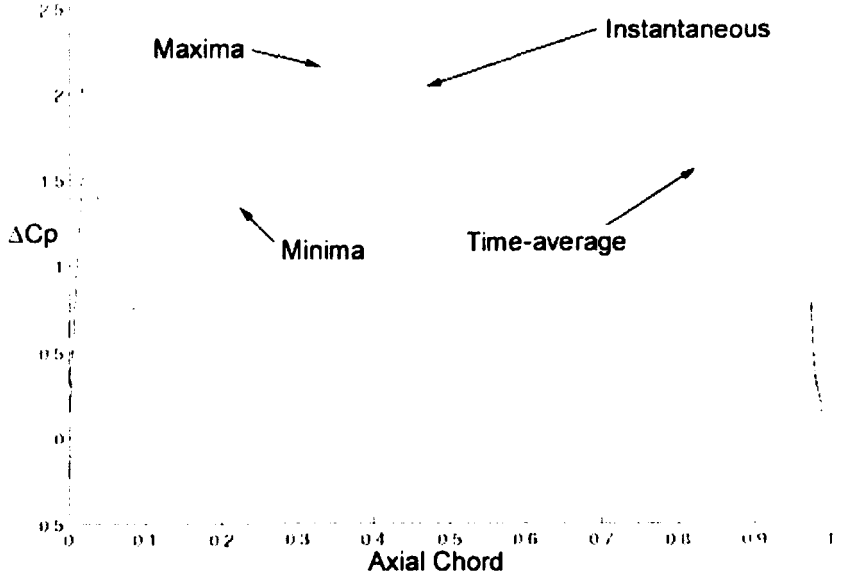

Figure 4-14: Time Analysis of ΔCp profiles on the blade section at 99% span. Minimum, Mean and Maximum ΔCp profiles are shown. A profile at a given instant is also represented.

of excitation, however its amplitude is much stronger on the PS than on the SS. LVCF is also observable in the vicinity of the leading edge, but it is two order of magnitude weaker than TVF. The second harmonic of TVF and modulations of TVF and LVCF can also be identified.

The difference of pressure across the tip of the blade is shown in Figure 4-14 , while Figure 4-15 shows the associated power spectrum. Locally higher ΔCp regions can be seen, they corresponds to the high-pressure spots observed previously on the PS and have been observed to also move along the tip.

It is anticipated that a fluctuating pressure difference at an axial position across the tip of the blade should naturally have an impact on the local tip leakage mass flow, as it is the driving force behind the tip gap flow. An increase in tip leakage mass flow - local jets - was observed in the tip gap locations corresponding to regions of higher ΔCp. The frequency analysis of the tip clearance mass flux in the tip gap give a plot very similar to the spectrum of ΔCp in Figure 4-15 .

Several remarks can be made on this spectrum:

- the dominant frequency is clearly TVF at all axial position

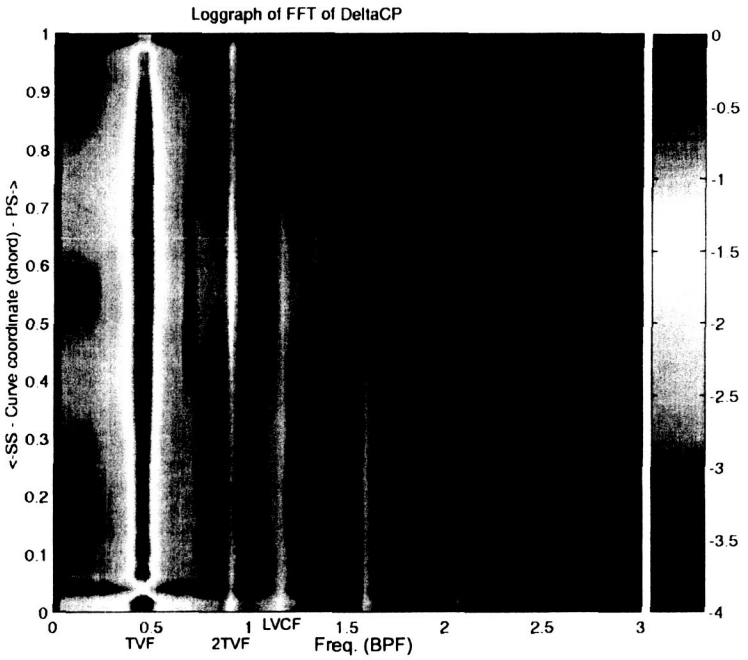

Figure 4-15: Power Spectrum of ΔCp at 99% span on blade surface

- the unsteadiness of the tip clearance flow is greater downstream of 40% and not at the onset of tip vortex formation

- very low frequencies of the order of 0.2 BPF were observed at two specific locations: 40% and 70%. The insufficient accuracy of our computations have not allowed further investigation.

This section presented computed results to delineate a series of flow events that are associated with the unsteadiness of the tip vortex flow. Wave-like pattern on the interface (between tip clearance flow and core flow), higher pressure regions on the PS of the blade and a local tip leakage jet proceed downstream in a spatially-synchronized fashion at a frequency corresponding to that of TVF. As the tip flow region grows in proceeding downstream, it induces a spot of higher pressure on the PS of the blade, the locally increased ΔCp across the blade tip implies a locally stronger tip leakage mass flow. This jet then interacts with the tip flow in the next passage, creating the wave-like flow pattern described herein above. The dynamic head of the tip leakage jet thus appear to be the cause of the increased pressure spot on the PS of the next blade.

However, the description of all these observed events does not provide a way to distinguish the causes from the consequences. They appear to be more like a loop of events, and the cause of the tip flow instability still remains elusive at this stage.

4.1.5 Forced Response of Downstream Wake

Beyond the effect of TV instability on the local rotor, the wake generated by the rotor also has an unsteady component associated with the tip vortex unsteadiness. Thus, the following question can be posed: Is TVF indeed observable in the rotor wake and what is its significance?

The analysis of the frequency content in the rotor wake shown in Figure 4-16 , proves that TVF is also a significant excitation of the rotor wake unsteadiness. It appears as the dominant frequency over a large span portion. In Figure 4-16 , positions of the pressure probes are at 4% pitch, 10% C_x behind trailing edge axial position, and 50, 75, 80, 85, 90, 95 % radial position (hub to tip). The time-resolved measurements are expressed in terms of pressure coefficient Cp. The evolution of the squared amplitude of the first two TVF harmonics is shown in Figure 4-16 (i). The ordinate is a logarithm of the square of the amplitude. The relative Cp variations are greater than 30% over 20% of the radial length of the wake.

The presence of TVF in the wakes has the implication that this excitation must be accounted for in the design of downstream bladerows. The designers might need to guarantee that such frequency of excitation will not endanger the integrity of the downstream blade rows of the compressor.

4.1.6 Summary

We have identified and characterized the tip flow instability as well as its implications in terms of blade forced response and rotor wake response.

The following points have been elucidated:

- under the conditions of our computations, an instability of the low-momentum tip flow has been demonstrated with a frequency equal to 0.45 BPF (TVF or a reduced frequency F_c^+ of 0.7)
- TVF is the dominant frequency in the tip flow region

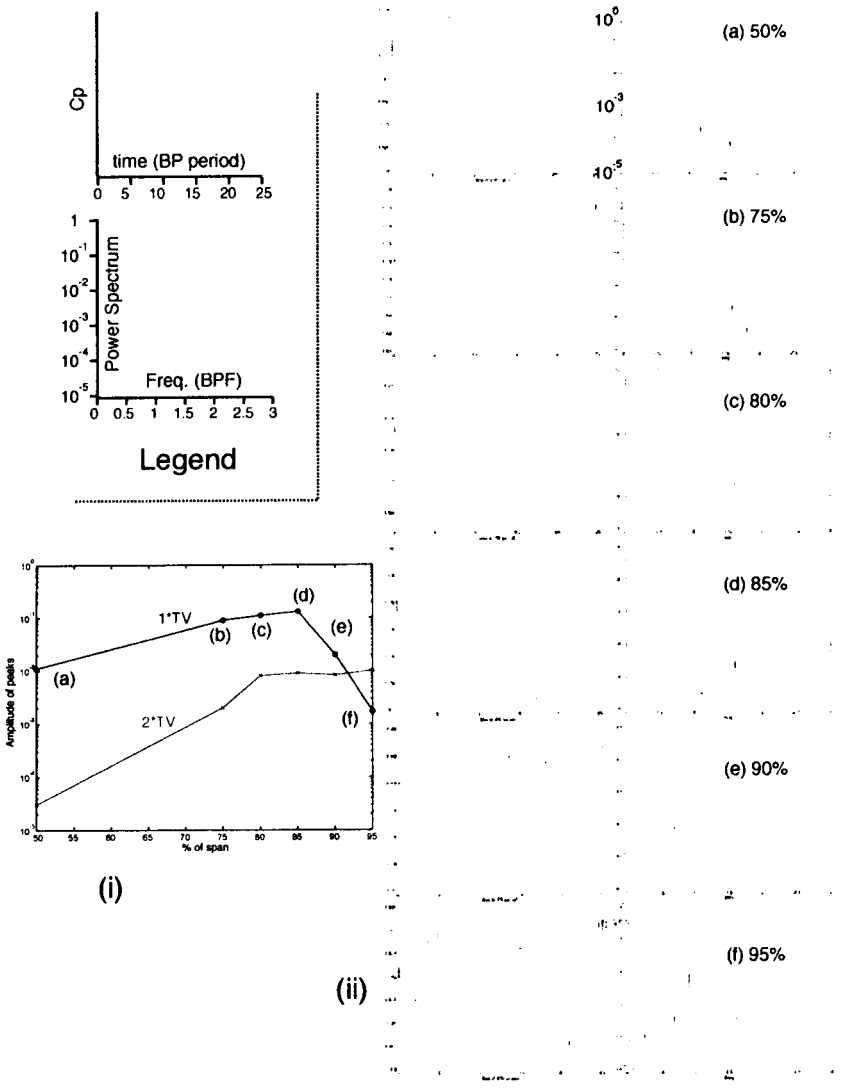

Figure 4-16: Series of static pressure probes and their corresponding power spectrum in the rotor wake. 0.1 chord behind the TE in the middle of the wake at different radial positions

- the vortical structure of tip clearance flow can only be identified in the first 40% chord region. Beyond that point, the tip flow is simply a low-momentum flow region, where there is no identifiable tip vortex structure.

- the tip vortex core, when it exists, exhibits motions at a frequency of LVCF equal to 1.15 BPF with no apparent relation to TVF. LVCF is only locally observed, always secondary and it is hypothesized not to be the cause of the tip flow instability

- the tip flow instability implies significant unsteadinesses on the rotor blade response as well as rotor wake response. It must be accounted for in the design of the rotor blade row as well as of the next blade rows

4.2 Wake-Tip vortex interaction in a Rotor

In the previous section, we have shown the significance of the self-induced instability of the tip flow on the blade forced response of a rotor blade row subjected to a uniform inlet flow. In an embedded multistage environment, the inlet flow consists of vortical disturbance.

In response to this, we can conceivably pose the following questions:

- Does the TV unsteadiness remain a relevant source of excitation when the rotor is subjected to strong wakes from upstream blade row? Does the TV unsteadiness persist? How does TVF evolves?

- How do the wakes and tip flow instability interact and what are the implications of this interaction for the designer in terms of aeromechanics?

4.2.1 Interaction of Wakes with Low-Momentum Tip Flow

In order to answer these questions, the tip and total blockage has been computed as a function of time and axial position, following the implementation as described by Khalid [11].

It is important to note that blockage computations in this thesis are not aimed at assessing the performance of the rotor, but rather at reliably determining the variation in the extent of the low-momentum flow region.

The interaction of wakes and tip vortex will be described based on the analysis of Figure 4-17 . This figure compares the contour plot of tip and total blockage for NW and SW. The

deviation of the local blockage to its time average value is actually shown on those plots.

$$\Delta Blockage(x,t) = Blockage(x,t) - \overline{Blockage(x,t)}^{t} \tag{4.4}$$

Blockage plots of the NW case are in the left hand column, while the right column is for the SW case. In all plots, the abscissa is time scaled to BP period. The TV period and overall convecting time $CT = \frac{C_{x,tip}}{U_{x,inf}}$ are also indicated on the x-axis. The ordinate is the axial position scaled by the axial projection of the chord length at blade tip Cx, tip. The first row of plots (ie. Figure 4-17 (a) and (c)) corresponds to the tip blockage plot.

In the NW case (ie. Figure 4-17 (a) and (b)), the tip vortex is the only source of unsteadiness, and both tip and total blockage show a clear TV periodicity. Waves of increased and reduced blockage convect through the passage. Since the blockage refers to a region of velocity defect, these waves can be thought of as variation from the effective time-average surface of separation between the tip flow and the core flow. While the period remains the same through the passage, the velocity of the wave-like pattern increases from a value of $V_1 = 0.28U_{x,inf}$ in the region up to $0.4 \cdot C_x$ range to $V_2 = 0.42U_{x,inf}$ beyond $0.4 \cdot C_x$. The former value is shown by the dotted lines, the latter by the dash-dot lines. $V_{1,2}$ is used here to denote axial component of the velocity at which the characteristic wave-like pattern of the tip clearance flow is moving. The subscript $_1$ is for the velocity near the inlet plane, $_2$ is for the velocity near the exit plane.

The primary perturbation in the tip region appears at 40% chord. It stands still while gaining amplitude before accelerating to V_2. The total blockage as shown in Figure 4-17 (b) does not show this perturbation, but pulses appear at the inlet plane of the blade passage accelerating from V_1 to V_2 progressively. The blockage were computed on axial cuts with no a priori consideration of the orientation of the structure of the wave-like pattern. The ratio of V_1 by V_2 is found to be equal - with a 4% error margin - to the ratio of the cosines of the mean flow angles at inlet and exit. This value is 0.65. This indicates that the orientation of wave-like pattern, which was observed to be orthogonal to the core velocity at exit. Again, core flow direction and patterns orientation seem to be closely linked.

It can be noticed that $U_{x,inf}$ is also observable in those plots, where smaller variations can often be seen to be propagating at $U_{x,inf}$.

In the SW case, strong wakes are input. Two specific features are observed:

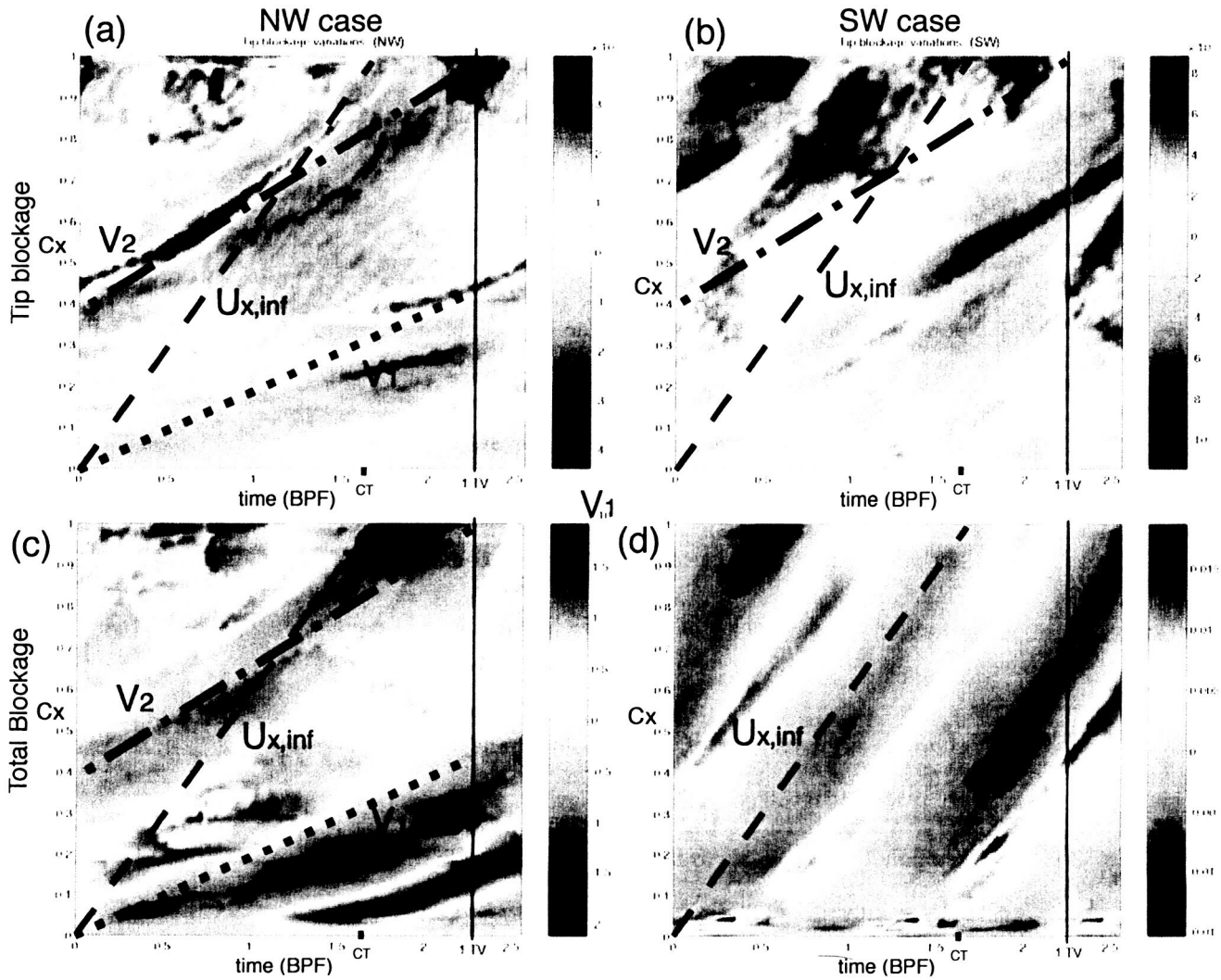

Figure 4-17: Comparison of tip and total blockage for NW and SW. In first row are tip blockage maps, total blockage graphs are in second row. Only the local variation of the tip and total blockage $\Delta Blockage(x,t)$ are plotted where $\Delta Blockage(x,t) = Blockage(x,t) - \overline{Blockage(x,t)}^{t}$

- The total blockage clearly show the influence of the wakes on the boundary layers. The variation in total blockage moves downstream at a speed equal to $U_{x,inf}$ which is approximately tha axial component of the velocity at which the wakes are convected downstream. It is not surprising as the wakes act to suck the BL fluid from the blade suction surface. No trace of any wave at V_1 or V_2 can be noticed. This was to be expected given the relatively high strength of wakes. But TVF is still present in an unexpected way: the amplitude of the blockage variation is modulated by as much as 80% at a frequency of TVF.

- the tip blockage plot for SW (Figure 4-17 (c)), on the other hand, show that TVF is still predominant in the tip flow region, despite the strong wakes in the core flow. The key point here is that the shape of the low-momentum region near casing is still driven by TVF.

In summary, three characteristic velocities are observable:

- the overall axial velocity $U_{x,inf}$, which corresponds to a displacement of $1 \cdot C_x$ for a CT period of time. It is denoted by the dashed lines.

- the inlet axial velocity of the wave-like pattern V_1 equal to 0.28 $U_{x,inf}$. It is denoted by the dotted lines.

- the exit axial velocity of the wave-like pattern V_2 equal to 0.42 $U_{x,inf}$. It is denoted by the dash-dotted lines.

Although the wakes are definitely the major disturbance for the entire blockage - due to their interaction with boundary layers - the TVF remains the primary frequency of disturbance in the low-momentum tip region.

4.2.2 Impact of TVF and Wakes on Blade Forced Response - Implication on Design

The examination of the low-momentum flow features in the tip region suggests that TVF is nevertheless dominant.

What is the impact of the coexistence of two independent disturbances such as wakes and tip vortex instability on the blade forced response?

Spectral analysis of the pressure coefficient at three different locations on the PS of the rotor have been carried out for SW as shown in Figure 4-18 .

The results indicate that:

- TVF and BPF are of comparable amplitude. TVF is clearly a major component of the blade excitation.
- the blade forced response contains a wide variety of frequencies. Most of them are identifiable as due to modulations of TVF and BPF, and thus cover a broad band.

The modulation BP-TV, TV and all increment of BP-2TV, plus 3 harmonics of BP, 2BP+TV and 3BP-TV are observable. The latter modulations are less noticeable at 70% axial chord: the spectrum mainly contains peaks at TVF, BPF and its harmonics, still 2BP+TV and a low frequency component at BP-2TV or 2(BP-2TV) are observable. TVF seems to exhibit a decreasing amplitude as we proceed downstream.

The array of new frequencies observed in the tip flow, is also found on the blade surface near the blade tip as shown in Figure 4-19 . As a consequence all the modulations of TVF and BPF described above are frequencies that designers might have to account for as non negligible excitations, whose effect could be of relevance. Again, we need to keep in mind that these 'unexpected' frequencies only exist because of the presence of the tip vortex instability, which interacts with BPF peaks due to wakes coming in. It might also affect design in the next blade rows, since this array of excitations is present in the rotor wakes and thus transmitted downstream, as shown in Figure 4-20 .

Discussion on Plausible Origin of TV Instability

So far, the analysis of the computed results have shown that the motion of the tip vortex core could not explain the frequency TVF observed in the tip flow region (section 4.1).

Furthermore, the followings have been measured:

- the wave-like structure of the interface separating the tip flow and the core flow proceeding at a TVF rate
- the increasing amplitude of variations in the interface in the downstream direction

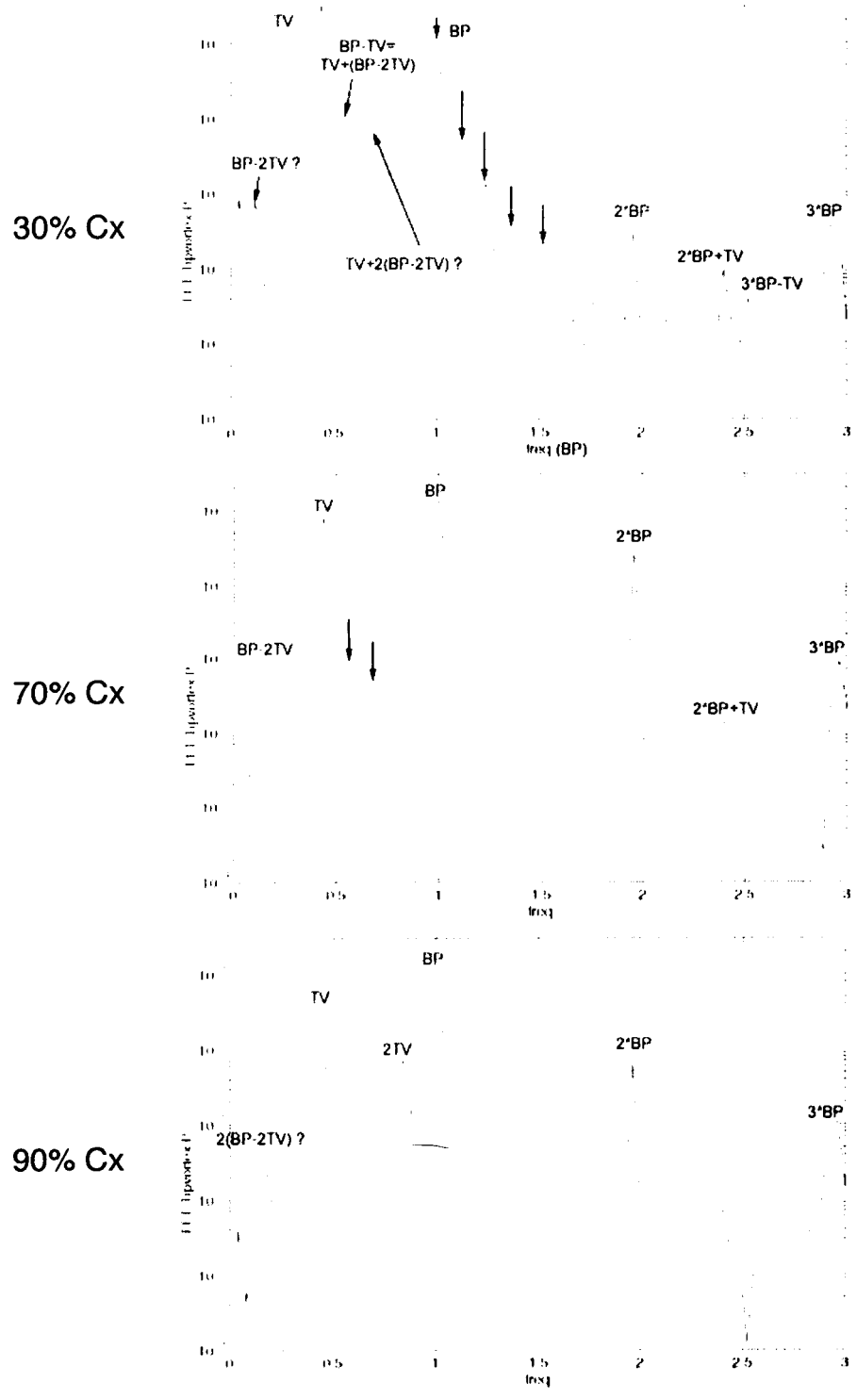

Figure 4-18: Power spectrum of Pressure coefficient at three axial position in the TV for the SW case. Probes are at 50% pitch, 95% span.

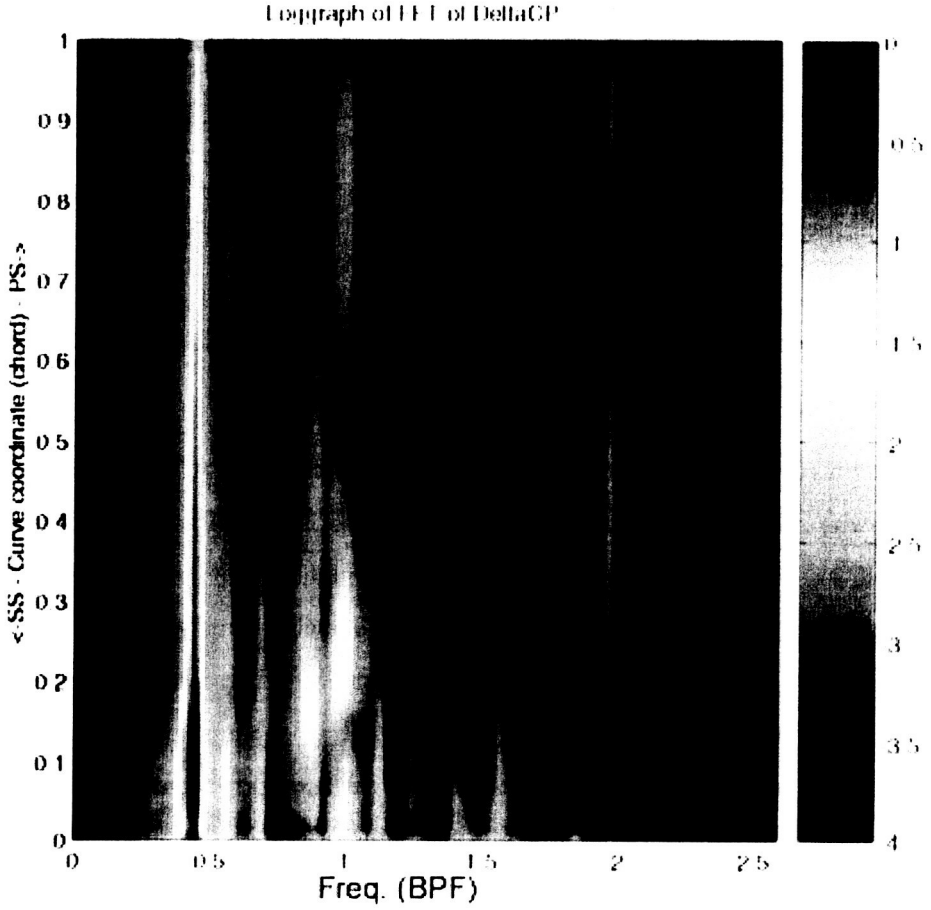

Figure 4-19: Power Spectrum of Delta Cp at 99% span across the tip gap

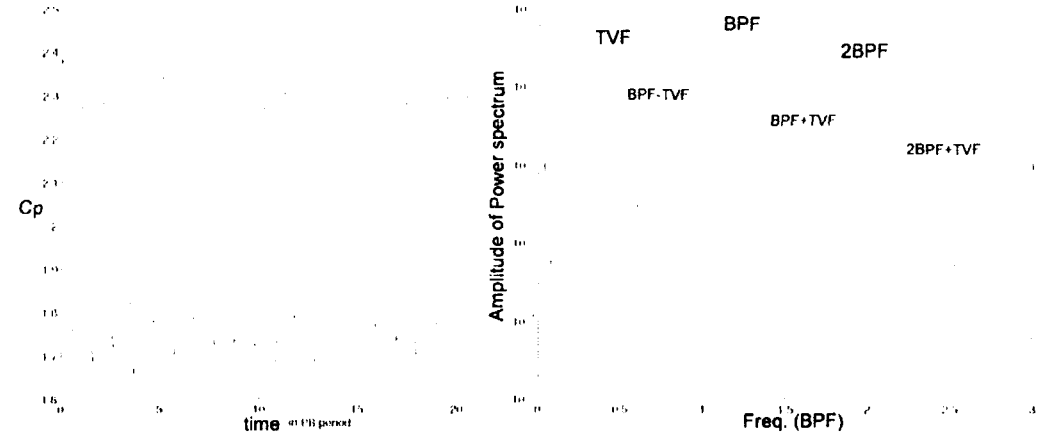

Figure 4-20: Power Spectrum of a pressure probe in the rotor wake at exit. Position of probes are 10% C_x behind rotor trailing edge in the middle of rotor wake, 90% span.

- the apparent close link of the spatial orientation of this variation with the core velocity direction

These observations suggest that the interaction of core flow with the low-momentum region might be the cause of the instability. This interface is indeed a zone of high shear and it is reasonable to think that the tip flow unsteadiness might be due to the shear layer structure.

The value of TVF remains to be explained. Following our hypothesis, we know the speed of the variation of the interface. In order to correlate this velocity of the variation to the time frequency TVF (reduced frequency F_c^+ of 0.7), an explanation of the wave length $\lambda_{TV} = U_{TV}/TVF$ of the wave-like pattern in the tip flow is necessary. Mailach [13] hypothesized that the periodical interactions of the tip clearance flow of one blade with the flow at the adjacent blade could explain that the instabilities rotate circumferentially. Vo [25] suspected that the source of the instability might be linked to a impinging backflow below the blade tip trying to propagate toward the leading edge while being held back by the incoming flow.

Further investigation of such conjectures might help determine the typical length scale of the wave structure observed on the interface. It should be noted that our single-passage numerical computations - implying a forced circumferential periodicity of the flow field - might have influenced the wave length of the wave-like patterns on the interface and therefore the value of TVF.

4.2.3 Summary

The post-processed results of a rotor blade row subjected to a steady wake in the stator frame has shown the relevance of considering the tip vortex instability as a major source of blade excitation. It has been observed that this instability is the disturbance that still drives the extent of the low-momentum flow region, despite the large disturbance brought by wakes to the system. This has confirmed that the temporal and spatial variation in the interface between the tip flow and the core flow has a close relation to the TV instability. It was shown that the wave-like pattern of the interface is oriented orthogonally to the core flow velocity. Hence, it is hypothesized from the present set of numerical simulations that the high shear at the interface could be the cause of the instability rather than the tip vortex structure as hypothesized by Bae [1].

The analysis of the rotor blade response has shown that TVF and BPF coexists and interact to produce modulations of lower and higher frequencies. Much like the phenomenon observed for the stator (Chapter 3), nonlinear effects have broaden the spectrum and the new high frequencies have a significant impact on the rotor blade excitation. On the contrary, the BPF was found to be clearly overwhelming in the rotor wakes, however, the presence of TVF and modulations implies that these unexpected frequencies might also be considered as significant fluctuations of the wakes of downstream blade rows. The key implication of this is that designers can not consider the tip flow instability to be a secondary effect when a rotor blade row is subjected to strong incoming disturbances, such as wakes. The TV instability is a phenomenon that needs to be accounted for in the design of a compressor.

4.3 Influence of wake fluctuations on the tip vortex. Potential of Resonance

In our analysis of a rotor subjected to steady wake, the wakes downstream of the rotor contained significant unsteadinesses due to the incoming wake (BPF), the tip flow instability (TVF) and the consequence of their interaction (in the form of modulations). The blade row downstream of the rotor is thus subjected to an unsteady wake in the rotor wake.

By computing cases of a rotor blade row subjected to incoming wakes that contain sinusoidal fluctuations at different frequencies denoted FW, our objectives was to answer the following

Cases	SW	FW3	FW1	FW4	FW2
FW (BPF)	0	0.37	0.0.45	0.625	1
FW_c^+	0	0.586	0.69	0.99	1.58

Table 4.1: Frequencies and reduced frequency of all computed FWi cases

questions:

- How do wakes and tip flow region interact when FW equals TVF? Is a resonance effect observed for the blade forced response?
- Should fluctuation in wakes be considered in the design of compressor?

4.3.1 Comparison of flow characteristics and blade excitation for different frequencies of fluctuation of the incoming wakes - Identification of a resonance effect

The fluctuation embedded in the wake can be seen as a third distinct source of unsteadiness, with the tip flow instability and the wake itself. Our primary objective was to determine how the flow characteristics and blade excitation evolve as the frequency of fluctuation FW is increased from zero (SW case) to a value greater than TVF. Especially, the situation where FW equals TVF is examined since it could potentially trigger a resonance effect of the tip flow instability on the flow field.

The frequencies of fluctuation FW and the associated reduced form FW_c^+ of each case are given in Table 4.1 .

The following metrics are used to assess the effects of unsteady wakes on tip vortex behavior:

- tip (or total) blockage comparison. Implementation of blockage follows Khalid's method defined in [11]
- comparison of static pressure coefficient, defined as $\Delta Cp_{s-s} = \frac{Ps_c - Ps_b}{0.5 \cdot \rho_{inf} \cdot U_{tip}^2}$
- tip leakage mass flow ratio
- force coefficient F_{coeff}, based on the integration of pressure distribution from 68% span to tip of rotor blade:

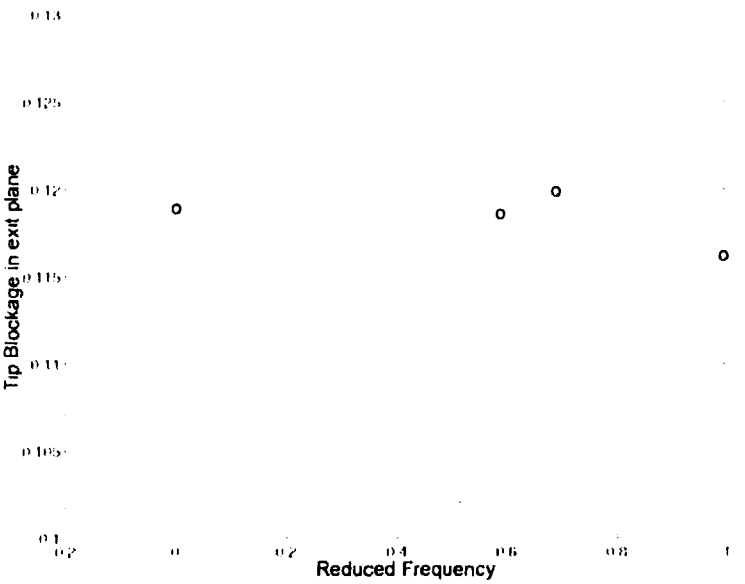

Figure 4-21: Comparison of Tip Blockage on the rotor TE exit plane

$$F_{coeff} = \frac{\int \int_{68\%span}^{tip} p \cdot ds}{0.5 \cdot Chord \cdot Span\rho \cdot U_{x,inf}^2} \tag{4.5}$$

Two types of comparison are made here:

- time-average values

- variability of values

Figure 4-21 , Figure 4-22 and Figure 4-23 show a comparison of tip Blockage, total blockage, ΔCp_{s-s} versus FWF, respectively. Time-average values are denoted with circles, while bars show the ranges of instantaneous oscillations.

In Figure 4-21 , we see that, on average, the tip blockage is greater when FW reduced frequency equals 0.7 -that is when FW equals TVF. The mean extent of the low-momentum tip region is thus increased when FW matches the TVF, suggesting that a resonance phenomenon between two disturbances of different origin - intrinsic TV instability and wake fluctuation - has occurred. The local peak is no more than 0.003 high, that is a 2% increase.

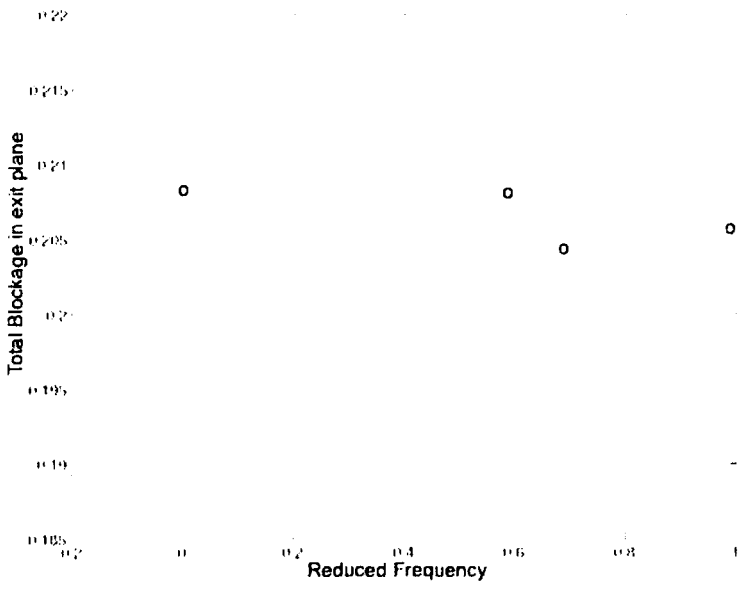

Figure 4-22: Comparison of Total Blockage on the rotor TE exit plane

On the contrary, the total blockage exhibit a clear minimum when FW=TVF. The increased tip blockage is thus overcompensated by a significant reduction of 'non-tip' related blockage, which gives a 3% reduction of blockage in all. In both tip and total blockage, a steep variation between FW3 and FW1 is observable. It should be noted how large instantaneous variations are compared to the relatively small mean evolution of blockage with FW; this is not believed to jeopardize our previous observations, since these bars characterize instantaneous behaviors. Hence, the resonance effect appear to have an overall beneficial effect.

This beneficial effect is confirmed by the results in Figure 4-23 , the pressure rise coefficient is greater when $FW_c^+ = 0.7$.

While a more pronounced effect has been demonstrated at $FW_c^+ = 0.7$ for blockage and pressure rise coefficient, the synchronization of FW with TVF has had limited effect. It can barely be called resonance. It is even more obvious for the tip leakage mass flow ratio and force coefficient. FW seem to have virtually no effect on their time averaged value, while it can again be noted that the variability is reduced when FW equals TVF as shown in Table 4.2 .

While the time-average quantitative impact of FW is limited, the frequency content of the blade response is significantly altered by the value of FW as will be shown in the next section.

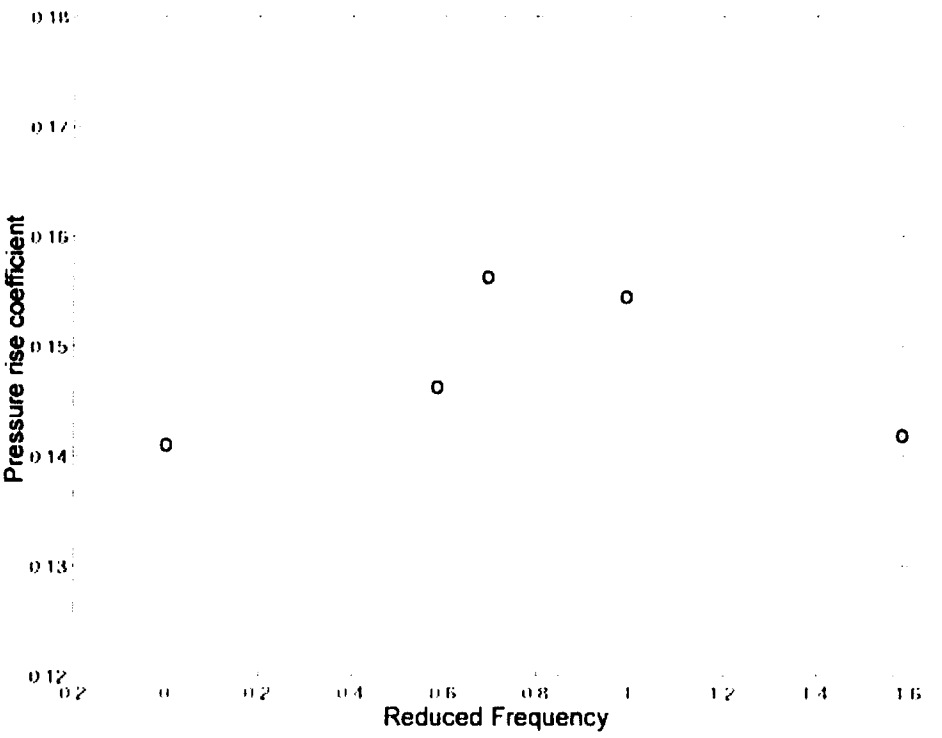

Figure 4-23: Comparison of the pressure rise coefficient

	SW	FW3	FW1	FW4
tip mass flow ratio(mean)	0.03	0.029	0.03	0.03
variability	7.5%	6.6%	5.85%	7.5%
Force coefficient(68%-tip)(mean)	1.43	1.419	1.42	1.42
variability	2.45%	3.5%	2.8%	3.2%

Table 4.2: Comparison of tip vortex mass flow ratio and Force coefficient computed from 68% to 100% span of the blade surface

4.3.2 Comparison of Frequency Content of the Rotor Blade Excitation

The frequency content of the blade excitation has been observed to be qualitatively dependent upon the value of the fluctuation frequency FW. The logarithm plot of power spectra of the ΔCp distribution along the rotor blade tip are shown in Figure 4-24 for four computations (SW, FW3, FW1, FW4). The abscissa of the plots is frequency normalized by BPF. The ordinate indicates the chord position.

The following points can be observed in Figure 4-24 :

- the FW3 and FW4 cases exhibits a much richer and enlarged power spectrum than FW1 and SW. This is consistent with the fact that FW3 and F4 are subjected to three main distinct disturbances frequencies - TVF, BPF and FW. The dominant frequencies (TVF, BPF and their modulations) are still very similar in amplitude to the case with steady wake (SW), but the amplitude of secondary frequencies between TVF(0.45 BPF) and BPF. Higher frequencies are also more important. This enlarged spectrum seem to be due to modulations of FW with the dominant excitation observed in SW.

- the FW1 case differentiates from the SW case, mainly by a new peak about $0.55 \cdot BPF$. This amplitude actually corresponds to BPF-TVF; the peak of BPF+TVF also has a higher amplitude than for the SW case, while the TVF peak has an amplitude equal to that in the SW case. The FW1=TVF fluctuation in the incoming wake seem to have just exacerbated the modulation of TVF with BPF, this might be related to the fact that the fluctuation FW is embedded in the wake.

The difference in frequency content is even more obvious for the force coefficient as shown in Figure 4-25 . In Figure 4-25 , the spectrum of the force coefficient (defined in the previous section) in the FW1 and FW4 cases are compared. The FW4 case exhibits a larger variety of dominant peaks such as those at BPF+FW4 and FW4. The FW1 mainly has only TVF, BPF-TVF and BPF as dominant excitations.

Hence, the frequency content of the blade forced response is very much dependent upon the value of the frequency of fluctuation of the simulated incoming wake. This has two major implications from the designer point of view:

- the unsteadiness embedded in the wakes is a relevant disturbance which has a noticeable impact on the extent of the spectrum of the blade response.

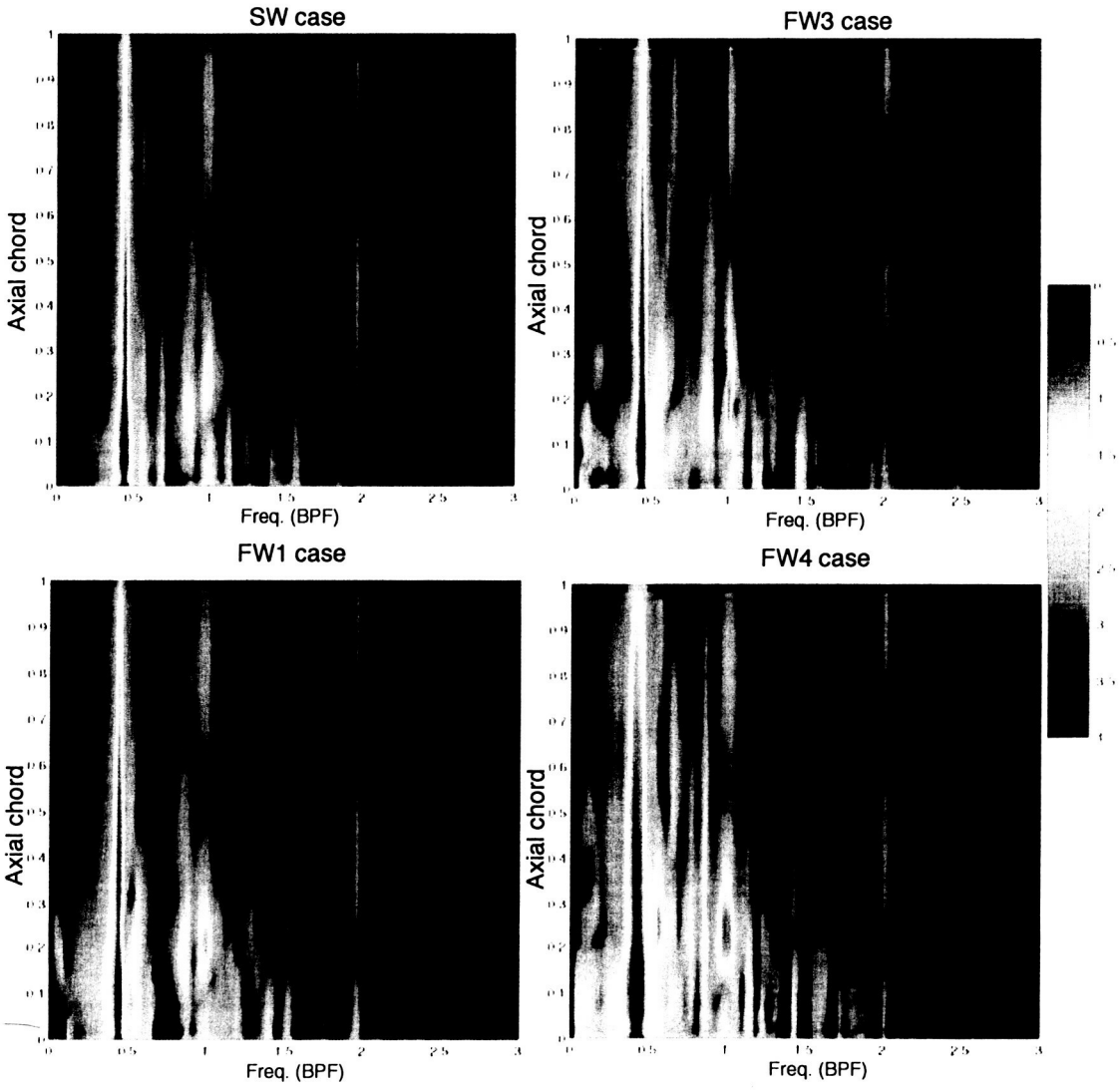

Figure 4-24: Comparison of Spectral analysis of the CP difference across the rotor tip at 98% span for the FW cases

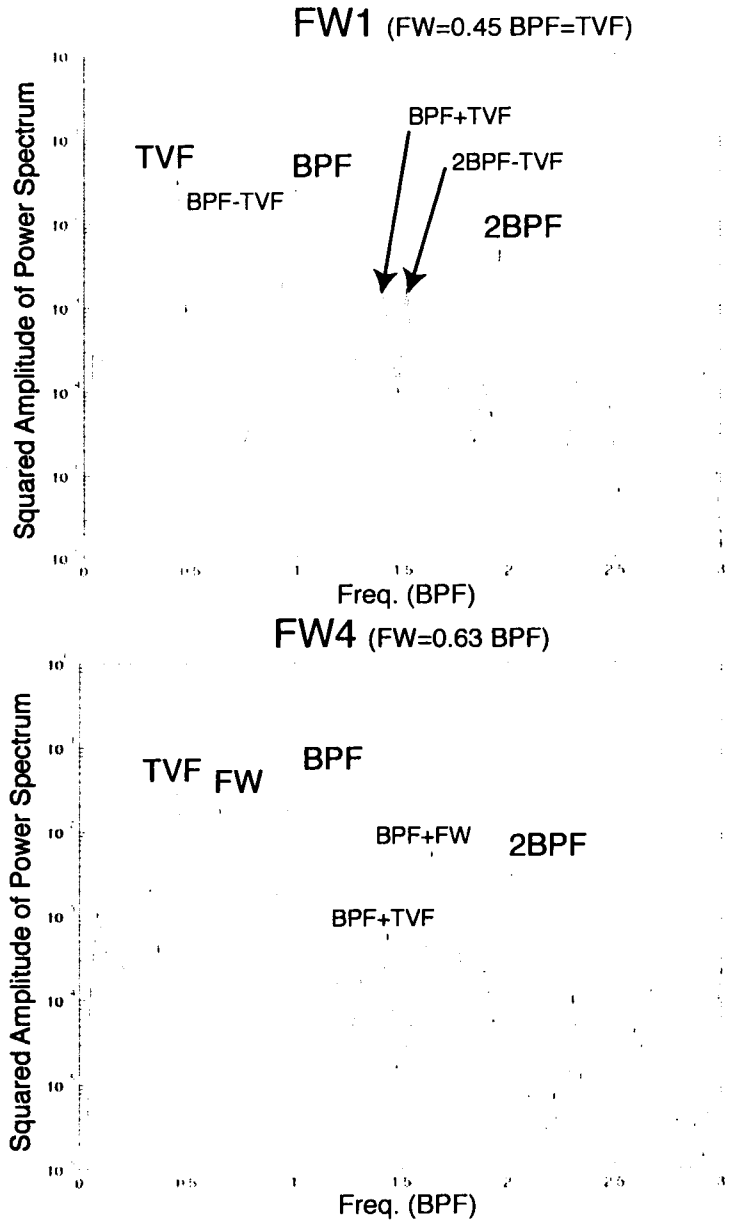

Figure 4-25: Power spectrum of the Force coefficient in the cases FW

- the spectrum of the wake fluctuation itself might have a critical role in the spectrum of rotor blade excitation

In the last section, we had observed that the wake generated by the rotor contained a variety of disturbances which are transmitted to the downstream blade rows. In this section, we have shown that such embedded disturbances have an impact in terms of frequency content on the blade forced response, such that it should be accounted for for robust design purpose.

4.3.3 Summary - Impact on the transmission and amplification of unexpected disturbances

Postprocessed results of a rotor blade row subjected to unsteady wakes containing a sinusoidal disturbance of adjustable frequency FW in the stator frame have shown that an overall beneficial effect in terms of blockage reduction and pressure rise coefficient could be observed when FW equals the tip flow instability frequency TVF. A disturbance in incoming wakes such as that implemented herein at FW=TVF does not imply a resonant effect on the amplitude of the tip flow instability in the tip region; this is presently attributed to the lack of correspondence between the spatial model structure of the unsteady wakes and that of the tip vortex instability. The frequency content of the rotor blade response however has been found to be dependent upon the frequency of the third independent fluctuation that is the wake fluctuation. For that reason, it appears critical that design processes should take into account:

- the fact that wakes are unsteady
- the frequency content of wakes which is closely related to the frequencies of unsteadinesses of upstream blade rows

in order to better predict blade forced response.

Chapter 5

Summary and Conclusion

5.1 Summary of Results and Conclusions

This study investigated the effect of interaction between tip clearance flow, steady and unsteady upstream wakes in rotor and stator blade rows in terms of blade forced response.
In a stator blade row, the interaction of steady wakes in the upstream rotor frame with the stator imply a blade forced response whose spectrum contains the Blade passing frequency (BPF) and its harmonics, with a decaying amplitude as the frequency increases. When the incoming wakes are unsteady, however, the spectrum of blade excitation exhibits unexpectedly amplified high frequencies due to the modulation of BPF with the fluctuation frequency.

In a rotor blade row, a tip flow instability has been demonstrated with a frequency (TVF) equal to 0.45 times the Blade Passing frequency corresponding to a reduced frequency (F_c^+) of 0.7.

Under uniform inlet flow conditions, the frequency and spatial content of the tip flow region have been characterized. The disturbance TVF was the dominant disturbance in the flow field and was found to imply variations of the pressure coefficient of more than 30% on the blade tip (between 35% to 90% chord) and in the rotor-generated wake (from 75% to 100% hub-to-tip position). In an attempt to better understand the origin of the instability, the structure of the tip flow has also been analyzed. The interface between the tip flow region and the core flow has been found to have periodical wave-like flow patterns which proceed downstream at a speed of approximately 0.42 times the core flow speed at a frequency corresponding to TVF. The

wave-like patterns in the tip flow region are associated with high pressure spots on the pressure side of the blade and a local jet in the tip gap. They all proceed downstream in a synchronized manner at similar speed. The vortical structure of tip clearance flow has only been identified in the first 40% chord region; beyond that point, the tip flow appears simply as a low-momentum flow region. Motions of the tip vortex core have only been observed at a frequency LVCF equal to 1.15 BPF (with no apparent relation to TVF) where the tip vortical structure is identifiable.

It is found that the tip flow instability is still the primary excitation on the rotor blade response, when the rotor bladerow is subjected to steady wakes in the stator frame. The interaction of the incoming wakes and the tip clearance flow induce an enlarged spectrum with high frequencies due to the modulation of TVF with BPF. An enriched spectrum is also observed in the rotor-generated wake and thus transmitted to the downstream bladerows.

If the rotor bladerow is subjected to unsteady wakes with a fluctuation at a frequency FW, a beneficial effect is observed in terms of performance when FW equals TVF. For any frequency FW, the spectrum of rotor blade excitation is enlarged by the interaction of the fluctuation with the two other primary disturbances (tip vortex instability and the incoming wakes). A modulation effect has generated new high frequencies excitations.

The following conclusions can be stated:

- the tip vortex instability can be a significant source of excitation of the blades. The wave-like structure observed on the interface between the low-momentum tip region and the core flow indicates that the origin of this instability could be related to the shear layer at the interface; this is in contrast to Bae's hypothesis that views the tip vortex instability as related to Crow instability observed in wing's trailing vortices. The frequency of motion LVCF of the tip vortex core is found to be unrelated to TVF and is always secondary - when observable. At this point, the physical cause of the instability and the reason for the value of TVF itself still need further investigations.

- the relevance of TVF as a primary component of the rotor blade excitation in the presence of strong inlet disturbances has been demonstrated. Given its intensity and its interactions with other inlet disturbances, the tip flow instability play a critical role in the broadening of the frequency band of the blade forced response.

- the effects of up to three major independent disturbances have been simulated in a rotor and stator blade row and their interaction have been found to produce a broad spectrum in the blade excitations and the downstream generated wakes as well. This has a major implication for the prediction of frequency content of blade forced response in a multistage environment, as unexpected high frequencies might persist many blade rows downstream.

- designers should consider the tip flow instability and its interactions with other inlet disturbances a key element in the prediction of blade forced response. In particular, the unsteady disturbances contained in the incoming wakes has proved to have a significant impact on the frequency content of the blade forced response. Hence, unsteady wakes containing the disturbances induced by upstream blade rows should be considered over steady wakes in design processes.

Empty page

Appendix A

Additional Comments on Rotor and Stator Computations

A.1 Estimation of the performance of the stage from the computed performance of the rotor alone

In this section all integrated values are mass-averaged on the axial cut corresponding to their position of specification (e.g. inlet or exit).

The purpose is to estimate what the static to stagnation pressure rise coefficient A.1 for the whole B Rotor/Stator of E3 would be, given our computed data for the rotor alone.

$$\frac{P_d - P_{Ti}}{0.5\rho_{inf}U^2} \tag{A.1}$$

where P_d is the static pressure downstream of hypothetical stator P_{Ti} is inlet stagnation pressure (known). U is the rotation velocity, ρ_{inf} is the inlet mean density.

Only P_d is unknown and need to be estimated. The following assumptions have been made:

- the axial velocity remains constant across the stator $V_{xc} = V_{xd}$
- for lack of good means to estimate it, we choose to estimate $T_c = T_d$. Hence the exit temperature of the stator is taken equal to the temperature at the exit of the rotor-only domain. This temperature is necessary to compute the sound velocity A.3.

- P_{td} is linked to P_{tc} using an overall loss coefficient $\bar{\omega}_d$ A.5 equal to 0.02, typical for an efficient blade profile [10].
- the flow mean angle δ_d at exit of the stator was computed from our complete rotor-stator computation 2. Its mean value was 37 deg., which is in very good accordance to experimantal measurements [21].
- γ is equal to 1.4

Given those assumptions, P_{td} is derived from A.5, V_d from A.4 and M_d from A.3. Finally, A.2 gives us an estimation of P_d.

$$\frac{P_{td}}{P_d} = \left(1 + \frac{\gamma - 1}{2} \cdot M_d^2\right)^{\frac{\gamma}{\gamma-1}} \tag{A.2}$$

$$M_d = \frac{V_d}{\sqrt{\gamma R T_D}} \tag{A.3}$$

$$V_d = \frac{V_{xd}}{\cos(\delta_d)} \tag{A.4}$$

$$\bar{\omega}_d = \frac{P_{tc} - P_{td}}{P_{tc} - P_c} \tag{A.5}$$

The obtained static to stagnation pressure rise coefficient for all our computations are compared in Figure 2-7 with the stage B characteristics from Silkowski [21] in the case of a 3.1% tip clearance. Despite the above assumptions, the estimated values stick close to the experimental curve.

Bibliography

[1] Jinwoo Bae. *Active Control of Tip Clearance Flow in Axial Compressors.* PhD thesis, GTL, MIT, June 2001.

[2] G.T. Chen, E.M. Greitzer, F.E. Marble, and C.S. Tan. Similarity analysis of compressor tip clearance flow structure. *J. of Turbomachinery*, 113, April 1991.

[3] W.N. Dawes. Simulation of unsteady blade row interaction with cfd: Applications. *Von Karman Institute Lecture Series*, Blade Row Interference Effetcs in Axial Turbomachinery Stages, february 1998.

[4] W.N. Dawes. Simulation of unsteady blade row interaction with cfd: Background. *Von Karman Institute Lecture Series*, Blade Row Interference Effetcs in Axial Turbomachinery Stages, february 1998.

[5] J. D. Denton. The use of a distributed body force to simulate viscous effects in 3d flow calculations. *ASME Paper*, 110, 1986.

[6] V. Girault. *Finite Element methods for Navier-Stokes equations: theory and algorithms.* Springer-Verlag, 1986.

[7] D.O. Gottliab and S.A. Orszag. Numerical analysis of spectral methods: Theory and applications. *SIAM*, NSF-CBMS Monograph, 1977.

[8] M. B. Graf. *Effects of Stator Pressure Field on Upstream Rotor Performance.* PhD thesis, MIT, June 1996.

[9] C. Hirsch. *Computational Methods for Internal and External Flows.* J. Wiley, 1988.

[10] J.L. Kerrebrock. *Aircraft engines and Gas Turbines.* The MIT Press, 1992.

[11] S. A. Khalid. *The Effects of Tip Clearance on Axial Compressor Pressure Rise.* PhD thesis, MIT, February 1995.

[12] K.Z. Korczak. *Development of an Issoparametric Spectral Element Mehtod for Direct Numerical Simulation of Navier-Stokes Equations.* PhD thesis, Dept. of Mechanical Engineering, MIT, June 1985.

[13] R.I. Mailach, L. Lehmann, and K. Vogeler. Rotating instabilities in an axial compressor originating from the fluctuating blade tip vortex. *ASME Paper*, 123, July 2001.

[14] J. Marz, C. Hah, and W. Neise. An experimental and numerical investigation into the mechanisms of rotating instability. *ASME Paper*, 2001.

[15] J. Marz, L. Neuhaus, W. Neise, and al. Circumferential structure of rotating instability under variation of flow rate and solidity. *VDI-Tagung:Turbokompressoren in industriellen Einsatz*, Oct 1998.

[16] L. Mongeau. *Experimental Study of the Mechanism of sound generation by rotating stall in centrifugal turbomachines.* PhD thesis, Pennsylvania State University, 1991.

[17] A.T. Patera. A spectral element method for fluid dynamics: Laminar flow in a channel expansion. *Journal of Computational Physics*, 54, 1984.

[18] J.S. Rao. *Turbomachine Blade Vibration.* John Wiley & Sons, 1991.

[19] S. Read and R. L. Elder. The nature of wakes in multi-stage axial flow compressors. *IMechE*, C557/100:545, 1999.

[20] E.W. Renaud. *Secondary flow, total pressure loss and the effect of circumferential distortions in axial turbine cascades.* PhD thesis, Dept. of Aeronautics and Astronautics, MIT, June 1985.

[21] Peter D. Silkowski. Measurements of rotor stalling in a matched and a mismatched multi-stage compressor. *GTL Report*, february April 1995.

[22] Theodore V. Valkov. Control of the unsteady flow in a stator blade row interacting with upstream moving wakes. Master's thesis, GTL, MIT, 1993.

[23] Theodore V. Valkov. *The Effect of Upstram Rotor Vortical Disturbances on the time-average Performance of Axial Compressor Stators.* PhD thesis, GTL, MIT, August 1997.

[24] Institute Van-Karman. Bladerow interactions in low pressure turbines. *Von Karman Institute Lecture Series*, february 1998, 1999.

[25] Huu D. Vo. *Role of Tip Clearance Flow on Axial Compressor.* PhD thesis, MIT, September 2001.

[26] Carlson Williams. Laser velocimetry study of stator/rotor interactions in a multi-stage gas turbine compressor. *J. of Turbo; AGARD*, 110:369, November 1988.

[27] D.C. Wisler and H-W. Shin. Blade row interaction and unsteady effects in axial-flow compressors and fans. *Von Karman Institute Lecture Series*, Blade Row Interference Effetcs in Axial Turbomachinery Stages, february 1998.

[28] AFOSR Workshop. Basic research issues in aerodynamics, structure dynamics and control of high cycle fatigue. *MIT Gas Turbine Laboratory*, October 1995.